FINAL REPORT

on

Gravity Gradient Stabilization System Elements and Antenna Structures

(11 June 1965 - 11 December 1965)

Contract No.: NAS 5-9598

Prepared by

WESTINGHOUSE DEFENSE AND SPACE CENTER

Aerospace Division

Baltimore, Maryland

for

GODDARD SPACE FLIGHT CENTER

Greenbelt, Maryland

Summary

The specific aim of this project has been to produce a rollable boom with windows in the boom walls and with interlocked seam edges, together with a deployer. The objective has been attained, and deliveries of test specimens and a deployer have been made. The delivered specimens have been three foot and ten foot lengths of three window areas and a solid wall tube. There have been two of each in each of the lengths making a total of 16 specimens. A deployer loaded with a ten foot boom has been successfully tested and delivered.

Analytical studies show that thermal deflections can be made to approach zero by optimum combinations of window areas and surface coatings. It involves the use of the unique window pattern, developed on this contract, which "averages" the exposure for all sun angles and the proper choice of surface coatings to balance the heat absorbed by both sides of the boom. It is indicated that a boom with window areas in the range of 10% to 20%, with a bright external surface, and with a dark interior surface will be a feasible design to minimize thermal bending.

Edge joining of the seam has been worked out to make major improvements in the torsional and bending characteristics of the boom. The deployer is adapted to "zippering" the seam as the boom is deployed. It functions for both pay-out and take-up.

Process development for making the booms from beryllium copper represents a major accomplishment of this project. Unique chemical milling, heat treating, and forming methods have been worked out and used with good results. It is clearly indicated that the process is applicable for continuous production of booms of indefinite length.

A production plan for making booms up to 1000 foot lengths has been submitted.

Table of Contents

		Page
	Summary	ii
	List of Illustrations	iv
1.0	Main Body	1
1.1	Introduction	1
1.2	Boom Analysis and Design	1
1.2.1	Problem Statement	1
1.2.2	Thermal Bending and Bending Strength	1
1.2.2.1	Requirements	1
1.2.2.2	Solutions for Window Patterns	3
1.2.2.3	Assumptions and Results of Thermal Analysis	10
1.2.2.4	Bending Strength	16
1.2.2.5	Conclusions and Summary of Thermal Bending Solution	19
1.2.3	Seam Design	22
1.2.3.1	Description	22
1.2.3.2	Torsional Rigidity and Strength	24
1.2.4	Thermal Bending and Strength Characteristics for Delivered Booms	24
1.2.5	Photographic Mask Preparation	27
1.2.5.1	Drawing	27
1.3	Material	28
1.3.1	Specification	28
1.3.2	Material Tests	28
1.3.3	Adaptation of Furnace to Material	30
1.4	Methods and Processes	32
1.4.1	Summary	32
1.4.2	Storage of Material	32
1.4.3	Cleaning	32
1.4.4	Coating	34
1.4.5	Mask Preparation	34
1.4.6	Printing	36
1.4.7	Developing	39

Table of Contents (Continued)

		Page
1.4.8	Chemical Milling	39
1.4.9	Final Cleaning	39
1.4.10	Tab Forming	42
1.4.11	Heat Treatment	42
1.5	Deployer	50
1.5.1	Introduction	50
1.5.2	Description of Design and Operation	50
1.5.3	Size and Weight	54
1.5.4	Material Considerations for Space	54
1.5.5	Test Results	55
2.0	Appendices	
	Appendix I	1-3
	Appendix II	1-10
	Appendix III	1-3

List of Illustrations

		Page
1.2.1	Orientation of Boom Relative to Direction of Irradiation	2
1.2.2	Window Pattern with Windows Located by Intersections of Longitudinals with Multiple Helix	5
1.2.3	Compound Helix Pattern for Random Shadowing	7
1.2.4	Shadow Patterns for Various Hole Patterns	8
1.2.5	Double Helix Showing Far-Side and Near-Side Lines Intersecting when Viewed Across Boom	9
1.2.6	Hole Spacing as Defined by Compound Helix	10
1.2.7	Holes on Orthoginal, Asially Oriented Grid	11
1.2.8	Temperature Profile Symmetry for $\alpha_o = A_w \alpha_i$	13
1.2.9	Relationship of Hole Spacing and Size on Conductivity	14
1.2.10	Experimental (by electrical analogue) Determination of k'/k	15
1.2.11	Bending Strength of Booms as a Function of A_w	20
1.2.12	Bending Strength of Booms per Unit Weight as a Function of A_w Normalized for Solid Booms	21
1.2.13	Edge Joining of Boom During Deployment	23
1.2.14	Bending Tester	26
1.3.1	Beryllium Copper Specimens Before and After Heat Treatment	29
1.3.2	A Stepped Cylindrical Mandrel for Application of Known Amounts of Bending Stress to Thin Strips	31
1.3.3	Tube Diameter and Stress vs Heat Treatment Temperature	33
1.4.1	Application of Photo Resist	35
1.4.2	Photographic Mask	37
1.4.3	Exposure Box	38
1.4.4	Developer	40
1.4.5	Etcher	41
1.4.6	Tab Bender	43
1.4.7	Heat Treater and Former	44
1.4.8	Continuous Heat Treater and Former	47
1.4.9	Heat Treatment	48
1.4.10	Boom Emerging from Heat Treatment	49

		Page
1.5.1	Deployer - Front View	51
1.5.2	Deployer - Side View	52
Appendices		
I-1	Variation of J, q and T with Length	2
II-1	Heat Flow for Elemental Strip	1
II-2	Coordinate System for Form Factor	2
II-3	Net Radiation from Interior Surface of Element dx	3
II-4	Net Solar Reflected Radiation Absorbed by Element dx	3
III-1	Superposition of Heat Flows for No Heat Flow at Seam	3

1. MAIN BODY

1.1 Introduction

Booms with window patterns to improve the thermal characteristics and with joined edges to improve the strength characteristics have been developed. A mathematical analysis shows how thermal bending can be minimized. Results of material studies show how beryllium copper can be processed to produce strong, straight booms. Processes for chemical milling, forming, and heat treating have been developed and used to produce booms which are being delivered to NASA for tests in a solar simulator.

The analytical study clearly shows that the use of appropriate surface coatings in combination with the window patterns, produced on this contract, will produce phenomenal improvements in thermal bending.

1.2 Boom Analysis and Design

1.2.1 Problem Statement

The two principal objectives of this design are: (1) to minimize thermal bending of booms by means of windows (or holes) in the boom walls and by the use of coatings with specific thermal radiation properties; and (2) to minimize torsional twisting of the boom by means of a seam with interlocking tabs.

The objects of the analysis are to establish the criteria for (1) determining quantitatively how much thermal bending and torsional twisting occurs for a specific design and environment; and (2) optimizing the design for a given task.

1.2.2 Thermal Bending and Bending Strength

1.2.2.1 Requirements

General Requirements

The main requirement is to minimize thermal bending of the boom; however, it is also important to maintain the bending strength

of the boom as much as possible. It will be shown in the solution that no trade-offs will be necessary here because a boom can be designed for absolutely no thermal bending with only a small loss in bending strength and stiffness. The radiation coatings should be stable for both the pre-launch, launch, and space environments for a reasonable length of time, and the boom must be capable of being deployed from the rolled-up condition into the tubular state and vice versa.

Thermal Requirements of Hole Pattern

The primary requirement of the hole pattern is to provide a relative distribution of radiation around the boom which is independent of the boom's orientation relative to the radiation vector; i.e., independent of β and θ (shown in Figure 1.2.1). This phenomenon will be called "averaging".

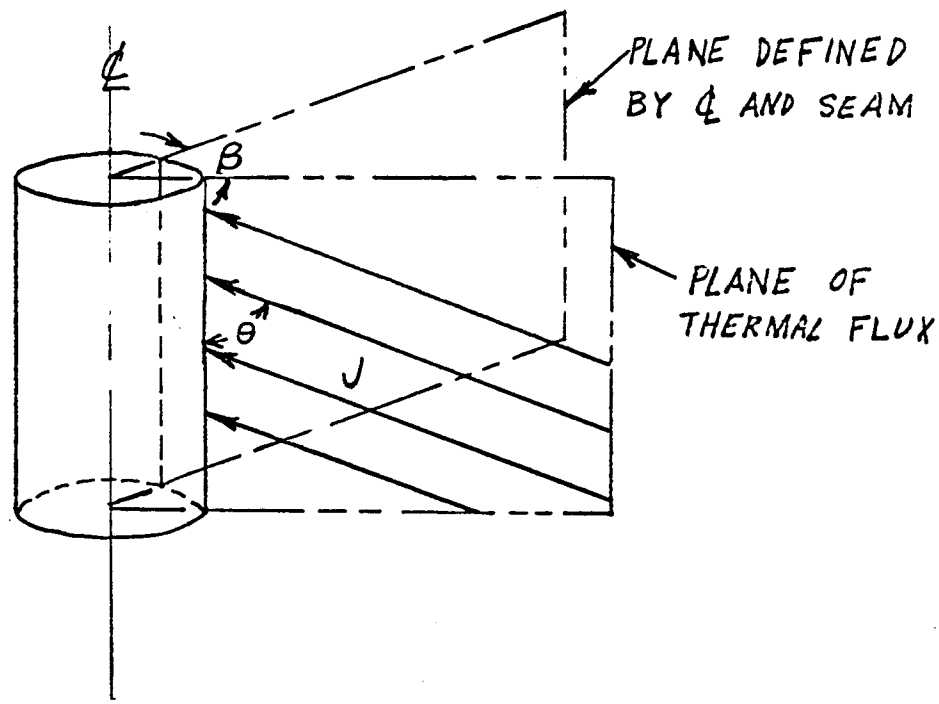

θ = angle between the ℄ of the boom and J vector which lies in the plane of thermal flux
β = angle between two planes shown

Figure 1.2.1 Orientation of Boom Relative to Direction of Irradiation

A secondary requirement of the hole pattern is that the thermal conductivity be degraded by the holes as little as possible.

Bending Strength Requirements

The existence of holes in the boom lowers its bending strength compared with a boom with solid walls. To minimize the strength loss, the holes should be as small and as few as possible within the limits of practicability; and the pattern of holes should be such as to maintain as much strength as possible. The actual strength required is of course dependent on the task, and the strength can be increased appreciably only by increasing the boom's diameter or thickness. For a given fractional window area, A_w, (the percentage of area of wall which is holes) it is better to have many small holes than a few large ones, because the strength is more uniformly distributed.

1.2.2.2 Solutions for Window Pattern

Evaluation of a Satisfactory Pattern

Four types of patterns have been considered in the search for one which "averages" the radiation. One is unsatisfactory structurally; two are unsatisfactory thermally, and the fourth is satisfactory both thermally and structurally. For purposes of documenting the investigation the three unsatisfactory patterns will be briefly explained since they were steps in the evaluation of the successful pattern.

The first pattern considered, but immediately discarded, is a random distribution of small holes. If there is a sufficient density of holes, significant variation in the irradiation distribution will statistically be confined to short lengths and the conductivity of the walls will smooth the variations to give some average value. However, the bending strength of the boom does not equal the strength of the average increment but of the weakest. Thus, this pattern is unsatisfactory structurally. Another disadvantage lies in the practical problem of making a random pattern.

A second approach to window pattern design is to have shadowing of the far side which varies predictably with orientation of the boom relative to the radiation vector. By using more than one surface finish on the inside in a particular pattern, the average heat absorbed by the far surface may be made to be a constant. This approach permits a uniform strength design. Considerable effort was made to achieve such a pattern, but without complete success. The most successful pattern discovered (see Figure 1.2.2) produces a thermal balance between near and far surfaces for rotations (β) about its axis, but has small deviations from perfect thermal balance for rotations (θ) in the plane defined by the radiation vector and the boom axis. Thus, thermal bending could be made small but could not be theoretically eliminated. (The qualification "theoretically" is made because even for a theoretically perfect pattern, some thermal bending will actually occur due to variations in surface finishes from the nominal values.)

A third approach to window patterns is to use a pattern that is stepped along the length of the boom, i.e., one that is rotated in the β direction at fixed intervals along the length. The idea here is that a pattern could be used which, for any angle β , would produce only local thermal bending, and that the net bending or deflection would be zero since one section would bend toward the sun and another away from the sun. The advantage here is that only one surface finish is required on the inside. However, problems are again encountered with rotations in the θ direction so that small deviations from an average thermal balance occur. Also, since the thermal expansion is proportional to the temperature T, whereas the emitted radiation is proportional to T^4, equal variations in heat irradiation along the length do not cause exactly equal expansions and contractions from the nominal length, thus causing some net bending.

A fourth approach to window pattern design is to produce a pattern that gives a random shadowing on the far side but that is actually not a random pattern. This design can therefore have a uniform strength while retaining the thermal advantages of a random pattern. To be effectively random for shadowing, the windows must be small enough that there can be a sufficiently large number around the circumference. This small size also allows less variation in temperature along the length because the conduction paths from hot to cold spots are proportionally reduced in length.

5773B-PF-1

Figure 1.2.2 Window Pattern with Windows Located by Intersections of Longitudinals With Multiple Helix

This random shadowing has been achieved by the design shown in Figure 1.2.3 on a flattened boom. The round holes are seen to be aligned on a slant in two directions. When the boom is formed, the result is two helices, one with a small lead angle and the other with a very large lead angle. The very large lead angle produces a random shadowing regardless of the orientation angle β, whereas the small lead angle produces a random shadowing regardless of the orientation angle θ. The result is that for any reasonable length (say, one diameter long), there is a constant ratio of the energy incident on the near surface to that on the far surface for any orientation of the boom. Therefore with proper surface finishes, thermal bending can be eliminated.

Considerations for Optimizing the Pattern

In presenting a successful type of window pattern, neither the helix angles, nor the hole sizes nor the hole spacings were defined. This is the task of optimization and practical compromise.

The dominant effect of the large lead-angle helix is on the wavelength of the shadowing pattern. This wavelength which can clearly be seen in Figure 1.2.4 should be kept small because it results in variations in irradiation and temperature of the far side of the boom. Unless the conductivity of the boom can smooth out the temperature variations sufficiently, the average thermal expansion of the far surface will not be the same as the expansion calculated based on the average radiation because, as explained previously, the thermal expansion is proportional to T, whereas the emitted radiation is proportional to T^4. For small variations of T from the nominal, the variation in emitted radiation is also proportional to T. The difference along the length for the pattern design selected (with a wavelength of 3/8") is less than 1/2°F as shown in Appendix I, so that its effect on bending is negligible.

The dominant effect of the small lead-angle helix is on the circumferential conductivity. This lead-angle should be kept small to increase the circumferential conductivity since this will minimize any thermal bending which may occur due to coating properties which are not

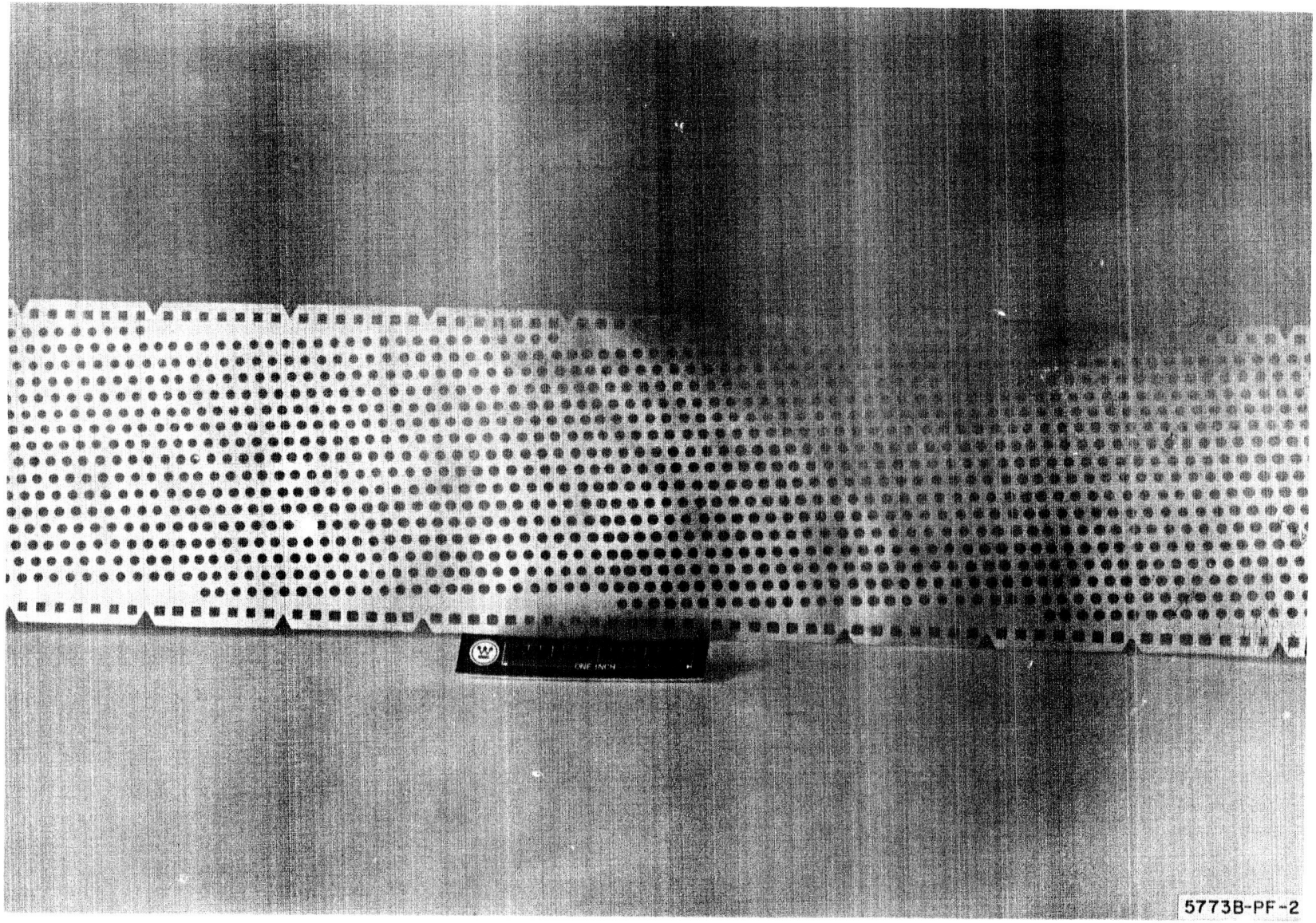

Figure 1.2.3 Compound Helix Pattern for Random Shadowing

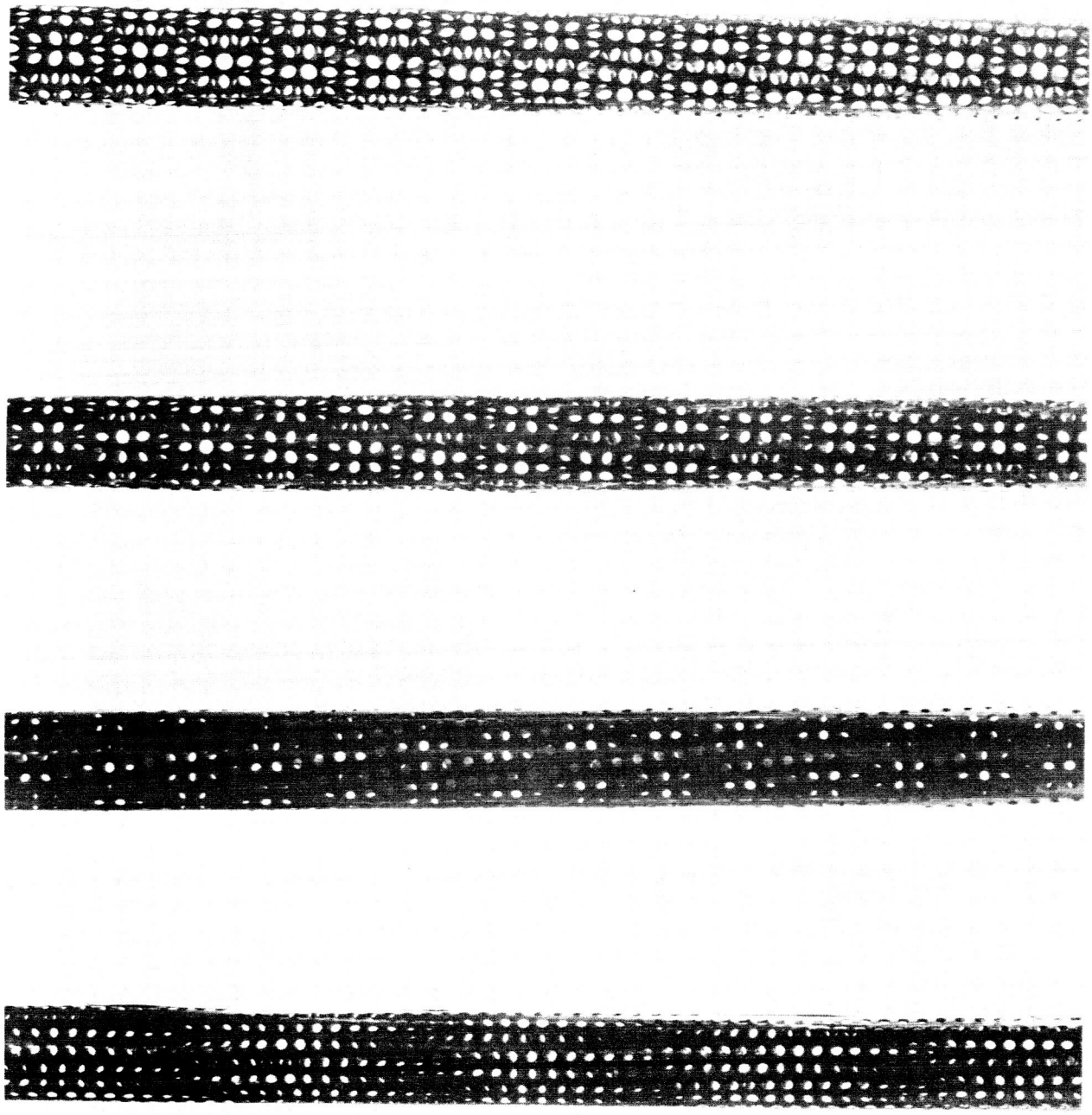

5773B-PF-3

From Left to Right

1) A_w = .25 , λ = 3/4 inch
2) A_w = .17 , λ = 3/8 inch
3) A_w = .33 , λ = 3/8 inch
4) A_w = .48 , λ = 3/8 inch

Figure 1.2.4 Shadow Patterns for Various Hole Patterns

optimum or to other anomalies. However, the lead angle must be large enough so as to result in at least a double helix, because the line of holes across the far side must cross the line on the front, when viewed across the boom, to give constant shadowing of the far surface as shown in Figure 1.2.5.

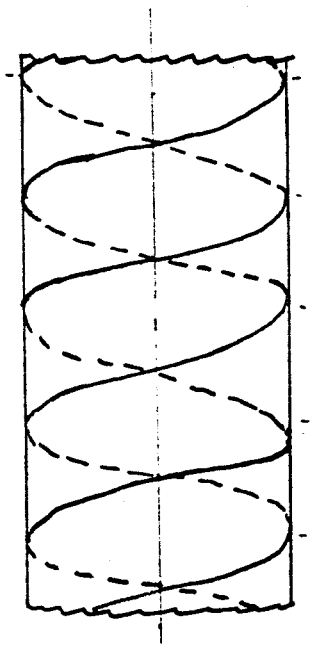

Figure 1.2.5 Double Helix Showing Far-side and Near-side Lines Intersecting When Viewed Across Boom

The hole size should be kept small for two reasons: (1) the strength of the boom is increased and (2) the hole spacing can be made smaller for a given A_w thus reducing the scatter in temperature from the nominal. The smallness of the hole is limited by two considerations. The first is that the diameter of the hole should be made considerably greater than the material thickness, otherwise the effective size of the holes becomes smaller as the incident radiation approaches grazing incidence and A_w is effectively decreased. If A_w is made larger to compensate, the gain in strength made by using smaller holes is lost. The second consideration is that manufacturing problems are increased because the mask is more complicated and the precision of the etching process becomes more critical.

Round holes have been used because they are much easier to fabricate, they result in minimal disturbances to the heat flow, and they cause the least stress concentration.

The hole spacing is dictated by the hole size, the fractional window area, and the angle between the intersecting helices (see Figure 1.2.6) according to the following relationship.

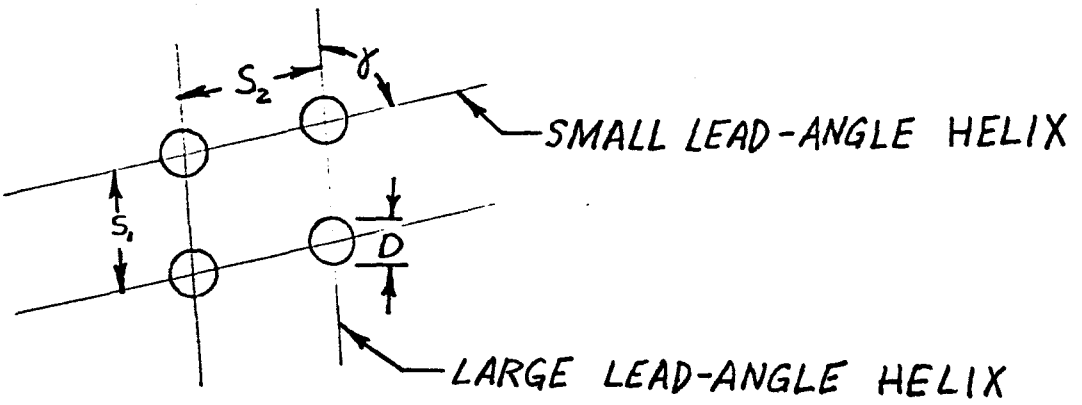

Figure 1.2.6 Hole Spacing as Defined by Compound Helix

$$A_w = \frac{\pi D^2/4}{S_1 S_2 \sin \gamma}$$

where A_w = fractional window area

D = hole diameter

S_1 = distance between holes on one helix

S_2 = distance between holes on other helix

γ = angle between helices

1.2.2.3 Assumptions and Results of Thermal Analysis

A thermal analysis is presented in detail in Appendix II. It derives the relationship between the window area and the radiation coating properties to eliminate thermal bending. It also derives an equation for the temperature distribution, the mean temperature, and the thermal bending radius for any combination of window areas and coatings.

The primary assumptions which were made and therefore those which limit the analysis are:

(1) the window pattern is one that "averages"

(2) the temperature variations of the boom's surface are small (say 10°F) so that every element radiates the same amount of energy.
Note: See Appendix I

(3) the inside surface coating reflects diffusely (according to Lambert's cosine law).

(4) the conductivity in the circumferential direction is the same at the seam as elsewhere.

(5) The thickness of the walls is considered negligible as regards shadowing.

(6) the effective conductivity, k', in the circumferential direction is the same as for a boom with holes on a square grid defined by axial and circumferential lines (see Figure 1.2.7).

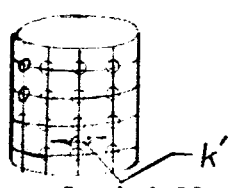

Figure 1.2.7 Holes on an Orthogonal, Axially-Oriented Grid

(7) the temperature does not vary along the length.

Some of these assumptions require justification.

The justification for number 2 is as follows: the temperature gradient around the boom is proportional to the heat flow and this is proportional to the radiated heat. The radiated heat is proportional to T^4 where T is the absolute temperature. Thus, a deviation of $\pm$ 5°F from the nominal for a typical boom temperature of 200°F results in an error of about $\frac{665^4 - 660^4}{660^4}$ or about 3% of this deviation, or .15°F.

The justification for number 3 is that the inside coating will normally be a dull black coating. This is usually very diffuse, and regardless of its diffusivity, the reflected radiation will be small and will have little effect on the thermal bending.

Number 4 cannot be well justified except that it is expedient for the analysis. However, if $\alpha_o = A_w \alpha_i$, the temperature gradients $\frac{dT}{dx}$ are very small so that the lack of conductivity across the seam will not be very large. The actual conductivity across the joint should be relatively good because of the elastic forces pressing the interlocking tabs of the seam together, and it should be much better than a simple overlapped seam. However, an accurate determination of the seam's conductivity will have to be determined experimentally in a vacuum. Every effort has been made in the design of the tabs to make the seam as tight as possible to aid thermal conduction. In Appendix III, the effect of absolutely no conduction across the seam is investigated.

Number 6 is easily justified for the existing design, since at the worst, k' would be multiplied by the cosine of the small lead angle which is about $\cos 10° \approx .99$.

The most important results of the analysis are:

(1) $\frac{1}{R_s} = \frac{er\,J_s}{2\,k't}\,(1 - A_w)\,(\alpha_o - A_w\,\alpha_i)\,\sin\theta_s$ for solar radiation

(2) $\frac{1}{R_e} = \frac{er\,J_e}{2\,k't}\,(1 - A_w)\,(\varepsilon_o - A_w\,\varepsilon_i)\,\sin\theta_e$ for direct earth radiation.

where:

R_s = radius of curvature due to solar irradiation (in)

e = coefficient of thermal expansion of boom material $(\frac{in/in}{°F})$

r = radius of boom (in)

J_s = solar radiation flux $(\frac{BTU}{hr\ in^2})$

k' = effective conductivity of boom material $(\frac{BTU}{hr\ °F\ in})$

A_w = fractional window area

α_o = solar absorptivity of outer surface

α_i = solar absorptivity of inner surface

θ_s = angle between boom axis and solar flux

R_E = radius of curvature due to earth radiation (in)

J_E = direct earth radiation flux $(\frac{BTU}{hr\ in^2})$

ϵ_o = emissivity of outer surface

ϵ_i = emissivity of inner surface

θ_E = angle between boom axis and earth flux

Therefore bending can be eliminated if

$$[3]\ \alpha_o = A_w\ \alpha_i \qquad \text{and}$$

$$[4]\ \epsilon_o = A_w\ \epsilon_i$$

The first of these is considerably more important since J_s is considerably greater than J_E. Since sunlight is reflected from the earth, for a boom near the earth this radiation must also be considered. The bend radius due to this will be given by [1] if the reflected flux is substituted for J_s. The net bend radius is simply the vector sum. It can be shown from the analysis that the temperature distribution is symmetrical about the two diameters perpendicular and parallel to the incident radiation as shown in Figure 1.2.8 if $\alpha_o = A_w\ \alpha_i$

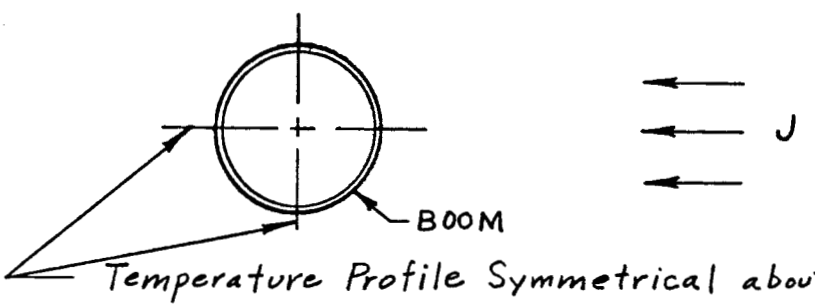

Figure 1.2.8 Temperature Profile Symmetry for $\alpha_o = A_w\ \alpha_i$

The conduction of heat around the boom is reduced by the holes in the boom wall. To determine the extent of this reduction, an electrical analogue was made to determine $C_1 = k'/k$, a constant which is a function of A_w. The term k' is the effective conductivity of an imaginary solid-wall boom of the same wall thickness which has the same circumferential heat conducting capability as the actual boom with holes. Assuming that the holes are located on an axially oriented square grid as shown in Figure 1.2.9, the following relationships can be stated:

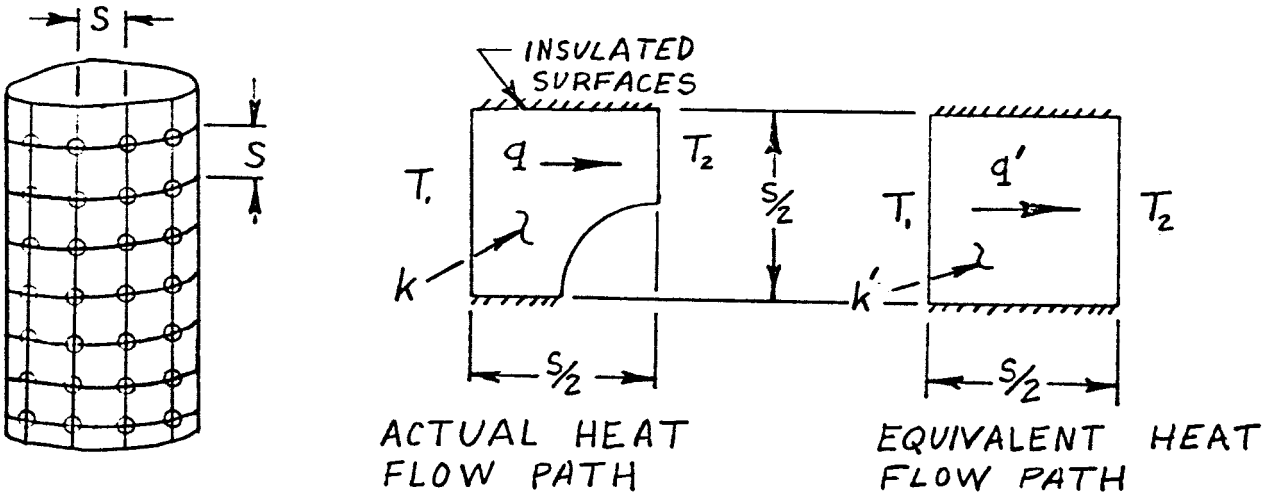

Figure 1.2.9 Relationship of Hole Spacing and Size on Conductivity

$$q = C_1 kt (T_1 - T_2) \quad \text{by actual heat flow path}$$

where q = heat flow per inch of width normal to flow direction $\left(\frac{BTU}{hr\ in}\right)$

C_1 = experimentally determined constant

k = thermal conductivity of boom material $\left(\frac{BTU}{hr\ ^\circ F\ in}\right)$

t = wall thickness of boom

$$q^1 = k' \frac{A}{L} (T_1 - T_2)$$

$$= k' \frac{S/2\ t}{S/2} (T_1 - T_2)$$

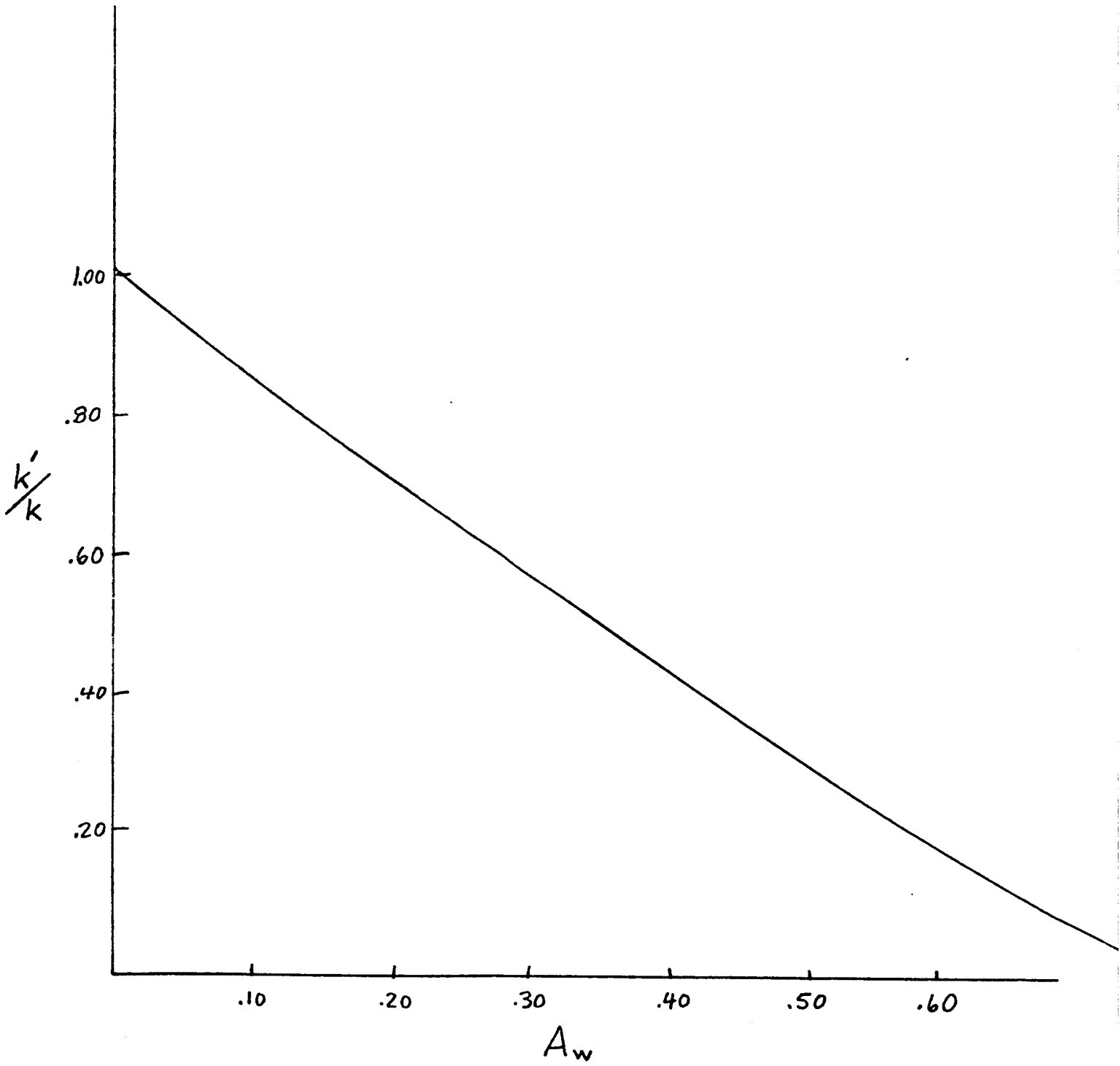

Figure 1.2.10 Experimental (by electrical analogue) determination of k'/k

$$q' = k' t (T_1 - T_2)$$

Since $q = q'$

$$C_1 k = k'$$

$$C_1 = k'/k$$

The constant C_1 was determined by graphical methods also, with very good agreement with the analogue results. The analogue results are given in Figure 1.2.10.

1.2.2.4 Bending Strength

The bending strength of the boom is somewhat less than that of a solid-walled boom of the same diameter, wall thickness and material. It is less because of the holes in the walls, the seam strength, and deviations from the perfect shape such as overall out-of-roundness, and local flatness due to forming processes. The buckling stress for a solid-walled seamless tube is given by

$$[5] \quad \sigma_x = \frac{\gamma E}{3(1-\mu^2)}\left(t/r\right) \approx .6\,\gamma E\, t/r \qquad 1$$

where

$$[6] \quad \gamma = 1 - .731\left(1 - e^{-1/16\sqrt{r/t}}\right) \qquad 1$$

For the design specified

$E = 19 \times 10^6$ (for Be. Cu.)

$r/t = \frac{.250}{.002} = 125$

σ_x = axial buckling stress (lb/in^2)

γ = correlation factor

E = modulus of elasticity (lb/in^2)

μ = Poisson's Ratio

t = wall thickness (in)

r = radius of boom (in)

1 NASA SP-8007, Sept. 1965, Eqs. 1.4.3.2-4 and 1.4.3.3-1

This gives for the buckling stress

$$\sigma_x = 57{,}800 \text{ psi}$$

The moment to cause this stress in a solid wall boom is

$$Ms_{cr} = \frac{I \sigma_x}{r}$$

[7] $$M_{cr} = \pi r^2 t \sigma_x$$

$$M_{cr} = 22.8 \text{ in-lb.}$$

Tests have been conducted on the existing patterns (from $A_w = 0$ to $A_w = .44$), and an empirical relationship which closely predicts the average buckling moment is

[8] $$M_{cr} = \frac{S-D}{S} M_{s_{cr}}$$

where

M_{cr} = buckling moment for any hole pattern, including solid wall booms

S = hole spacing

D = hole diameter

$M_{s_{cr}}$ = buckling moment for a solid-walled extendible boom

For S = .10, this becomes $M_{cr} = M_{s_{cr}} (1\text{-}10D)$

Since $M_{s_{cr}}$ was determined experimentally to be 14.5 in-lb.

M_{cr} is given by

$$M_{cr} = 14.5 (1\text{-}10D) \text{ in-lb.}$$

This is equivalent to saying that the crippling stress is a constant for all hole patterns since the maximum stress varies as $(\frac{S}{S-D}) \sigma_o = \frac{1}{1-10D} \sigma_o$ where σ_o is the stress on a solid boom. The scatter of

test results for the normal quality of production is indicated in Figure 1.2.11. For the existing designs, the seam is usually the weakest area, but in compression only. The average strength with the seam in compression is about 10% less than for other directions of bending, with the worst cases about 20% weaker. This could probably be increased somewhat by making the tabs shorter. To investigate the strengths of booms of equal weight, instead of equal wall thickness, consider the following: combining equations [5], [7] and [8] gives

[9] $M_{cr} = \gamma\, r\, t^2 \left(\frac{S-D}{S}\right)$ for constant wall thickness. The weight of a boom is governed by the following proportion

[10] Weight $\sim (1 - A_w)\, rt$

If r and t are allowed to change to maintain constant weight as holes are made in the wall

11 $r_1 t_1 = (1 - A_w)\, rt$

where the subscript 1 refers to a solid-walled boom. To maintain a constant flattening stress the ratio

12 $r/t = \text{const} = r_1/t_1$

Substituting for r from [12] into [11]

$$r_1 t_1 = (1 - A_w)\, r_1/t_1\, t^2$$

$$t_2 = \left(\frac{1}{1 - A_w}\right) t_1^2$$

Similarly

$$r^2 = \frac{1}{1-A_w}\, r_1^2$$

Substituting for [9] in r and t

$$M_{cr} = \gamma\, r_1\, t_1^2 \left(\frac{1}{1 - A_w}\right)^{3/2} \left(\frac{S-D}{S}\right)$$

Since $\gamma = f\ (r/t)$ and r/t is held constant

$$\gamma = r_1$$

$$(M_{cr})_{\substack{\text{const}\\ \text{wt.}}} = M_{s_{cr}} = \left(\frac{1}{1 - A_w}\right)^{3/2} \quad \frac{S-D}{S}$$

This function is plotted in Figure 1.2.11 as a dotted line.

If the booms are compared on a strength-to-weight basis, the booms of constant weight are slightly better than those with constant wall thickness. This is so because the strength per unit weight for constant wall thickness is

$$\frac{(M_{cr})_{\text{const } t}}{1 - A_w} = M_{s_{cr}} \left(\frac{S-D}{S}\right) \left(\frac{1}{1-A_w}\right)$$

$$\frac{(M_{cr})_{\substack{\text{const}\\ \text{wt}}}}{\dfrac{(M_{cr})_{\text{const } t}}{1 - A_w}} = \left(\frac{1}{1-A_w}\right)^{1/2}$$

This function is plotted in Figure 1.2.12.

1.2.2.5 Conclusions and Summary of Thermal Bending Solution

Since the solar radiation is dominant, the relation (from 3) $A_w = \frac{\gamma_o}{\gamma_i}$ is most important. Since the buckling strength varies as

$$\frac{M_{cr}}{} \quad 1 - D/S$$

$$\frac{M_{cr}}{} \quad 1 - 1.12 \sqrt{A_w}$$

even a small A_w results in a very significant decrease in bending strength. Thus to achieve good strength A_w should be minimized. Therefore γ_o should be minimized and α_i maximized. For practical coatings γ_o can be as low as about .07 and γ_i can be nearly 1.00. Therefore the minimum practical value of A_w is about .07. Two typical coatings might be silver on the outside and copper oxide on the inside.

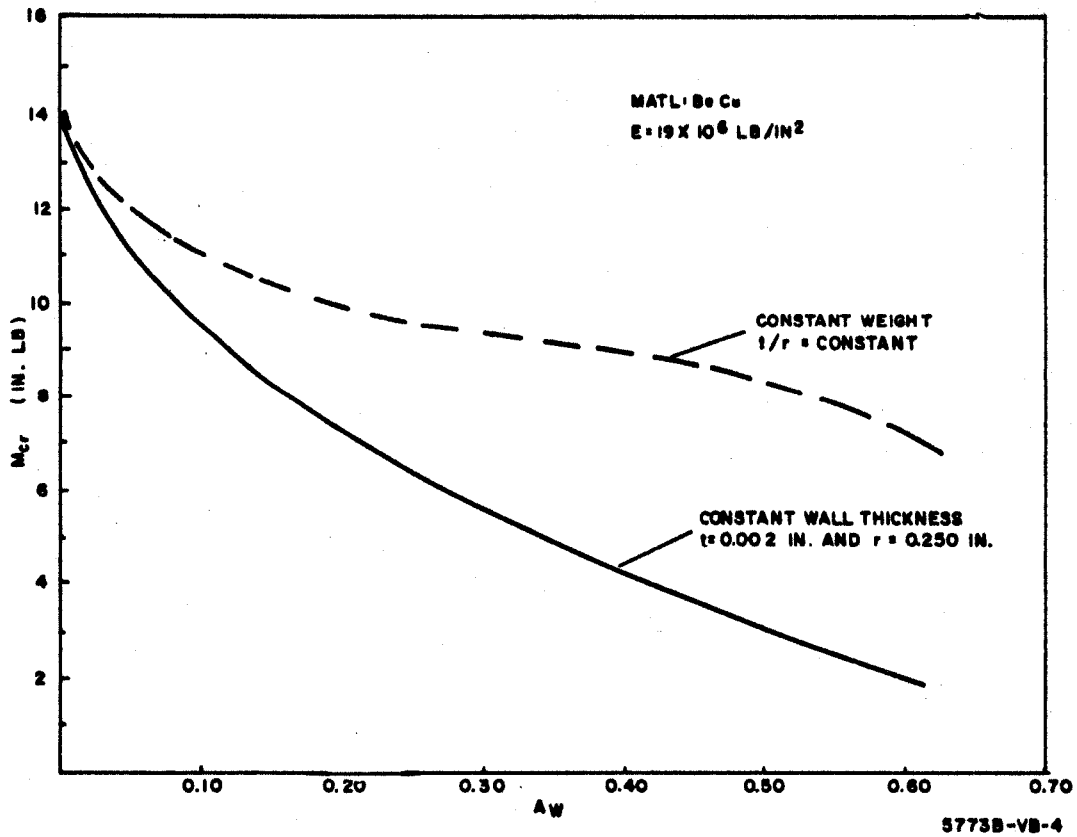

Figure 1.2.11 Bending Strength of Booms as a Function of A_w

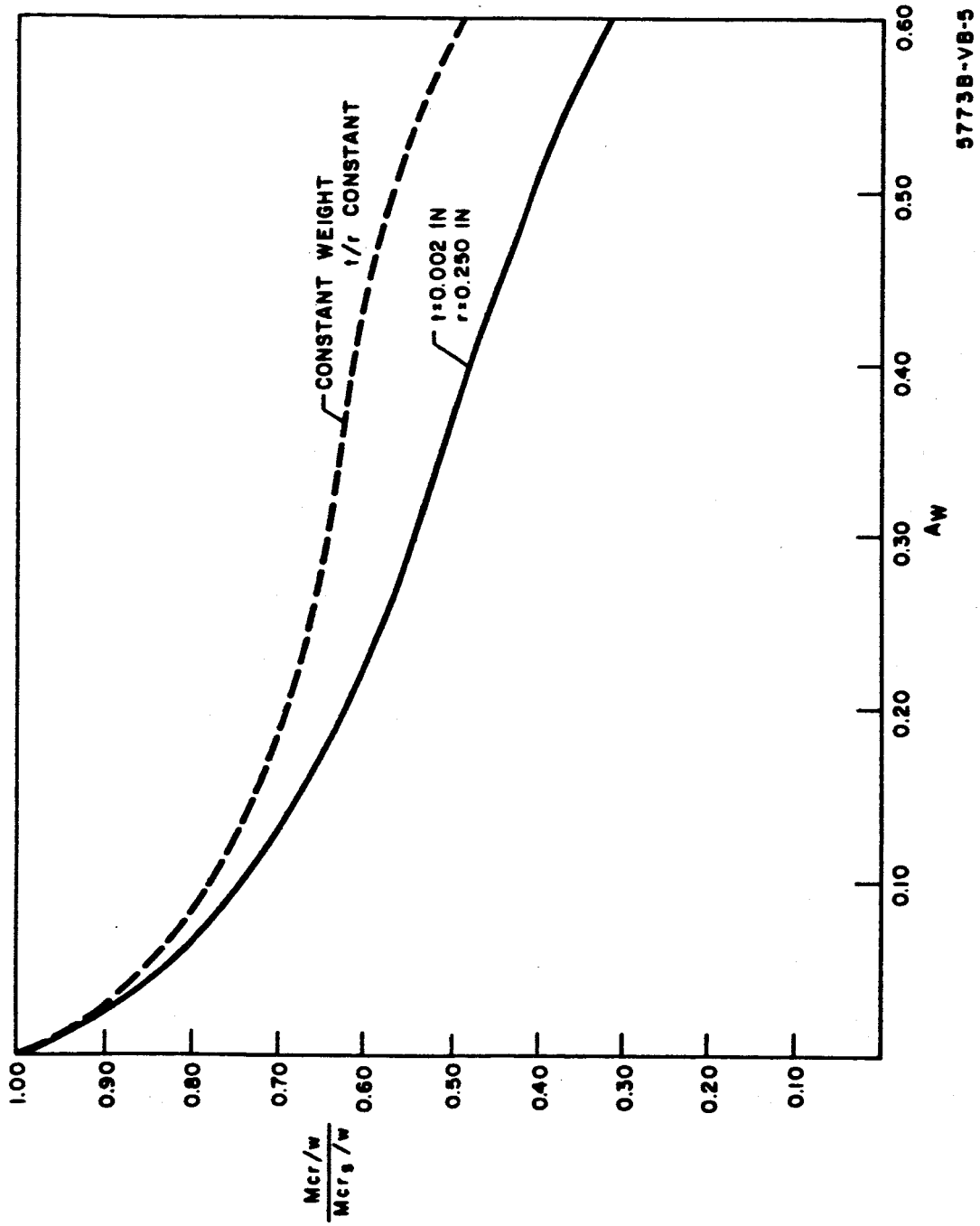

Figure 1.2.12 Bending Strength of Booms per Unit Weight Normalized for Solid Boom

To find a suitable set of coatings requires a great amount of research and testing. Since some bending can also occur because of the infrared direct radiation from earth, it is also desirable that $A_w = \frac{\varepsilon_o}{\varepsilon_i}$. Therefore, for the ideal set of coatings $\frac{\alpha_o}{\alpha_i} = \frac{\varepsilon_o}{\varepsilon_i} = A_w$. Since there is a manufacturing tolerance on α and ε, sufficient investigations on these tolerances would also be required to establish the optimum coatings.

1.2.3 Seam Design

1.2.3.1 Description

The edge joining can be seen in an erected boom in Figure 1.2.5, and the mode of engagement can be seen in a boom being formed from the flat in Figure 1.2.13. Each edge consists of tabs separated by notches. The notches on one edge engage the notches on the other. The tabs from one side alternately lap over or slip under the tabs on the opposing edge. The elastic energy of the boom forces the edges together (the boom is formed to a smaller radius than that which it has when joined). This alternate lapping feature guarantees continuity of bending stiffness and strength across the joint, and thus improves the bending strength for the mode of failure in which the boom flattens to produce buckling.

The greatest advantage of the joined edges over non-joined edges is for torsion. The interlocked edges carry the shear flow across the joint, thus giving the boom almost the stiffness of a closed tube which is many orders of magnitude greater than a slit tube. The torsional strength is also greatly improved.

The correct joining of the edges is insured by having alternate tabs more or less flat while the mating tab on the opposing edge is curved inward. Thus when the deployer brings the edges together, the flat tab overlaps the opposing inward-curved tab.

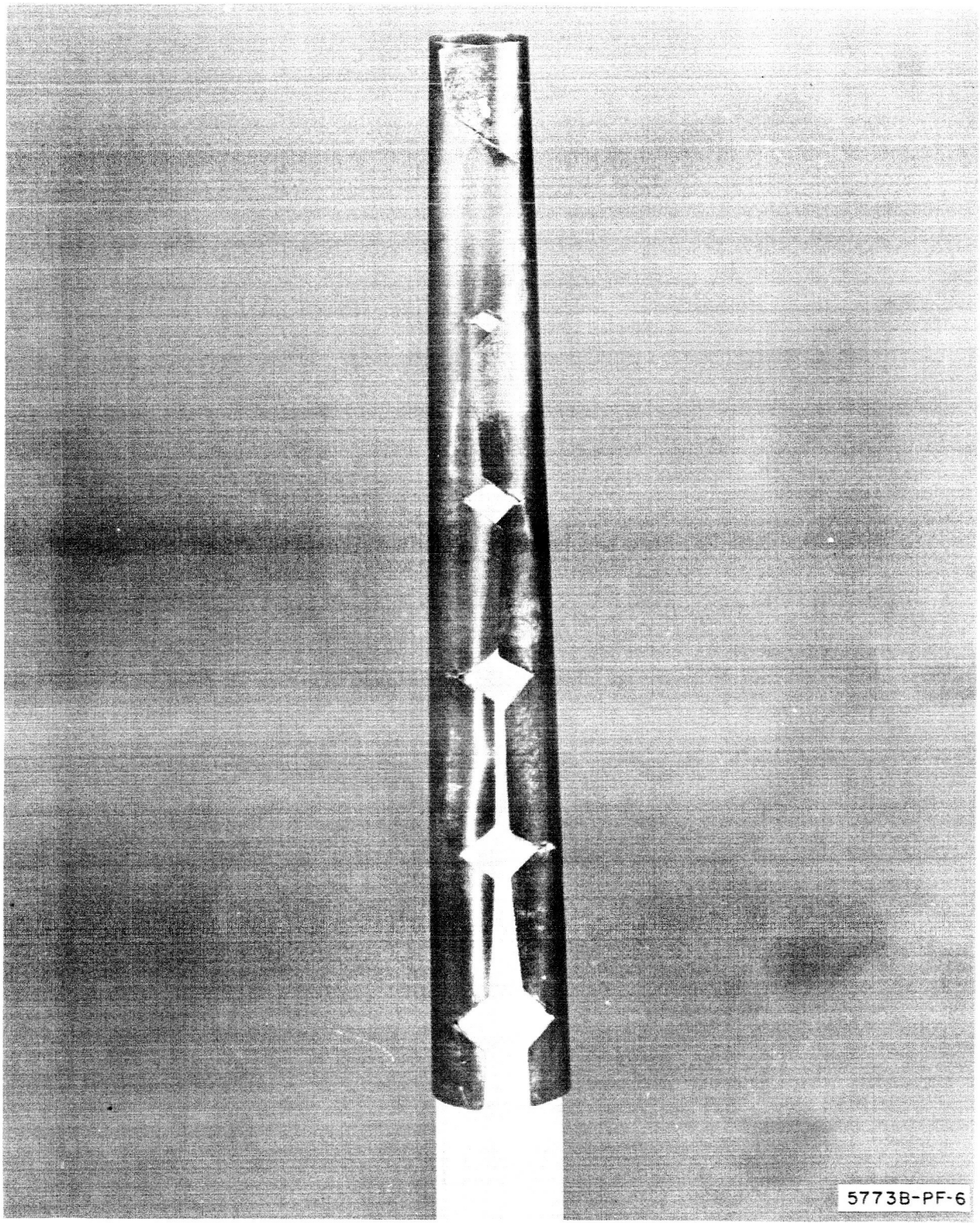

Figure 1.2.13 Edge Joining of Boom During Deployment

1.2.3.2 Torsional Rigidity and Strength

The torsional rigidity and strength requirements of a boom for a typical space task may vary over a wide range. Because of the seam design, the torsional strength and stiffness are less than that of a seamless boom. Since the shear strength of the seam is somewhat dependent on the number of interlocking tabs per unit length, this number is determined partly by the torque requirements. The number of tabs per unit length also affects the compressive strength of the seam. The existing seam design has 1 1/3 tabs per inch on each edge. This has been very satisfactory since the seam is only slightly weaker in the bending test than the rest of the boom, and it can easily carry the shear load due to the specified torque capability (.060 in-lb.). The existing design is not the optimum design for maximum torsional strength. The existing seam design also allows some non-elastic backlash in torsion when reversing the load direction, but a seam design could be made to eliminate this backlash.

1.2.4 Thermal Bending and Strength Characteristics for Delivered Boom

The delivered booms are made of unplated beryllium copper and do not realize the potential of the windows because they do not have the proper thermal radiation coatings prescribed by the relationship $\alpha_o = A_w \alpha_i$. Instead $\alpha_o = \alpha_i \approx .34$ and $\varepsilon_o = \varepsilon_i \approx .10$. The deflections of 30-inch long cantilevered booms with solar radiation (450 BTU/hr.ft.^{2}) directed normal to their axes, as predicted by equation 1 are shown below with mean temperatures, T_m:

A_w	$1/R^{(-1)}_{(in)}$	$\delta_{(in)}$	T_m (°F)
0	.000188	.085	272
.17	.000177	.079	224
.33	.000164	.074	245
.48	.000158	.071	254

With the prescribed coatings and reasonable manufacturing tolerances, this deflection could be held below .004 inches.

Tests were made to determine the bending strength and stiffness for booms with various window patterns, and to investigate the effect of the seam. Because of the possibility of non-uniform strength along the length and because of possible end effects, it seemed desirable to apply the maximum bending moment along the whole length so that any weakness in that length would be discovered. Hence a testing machine was built to apply a constant moment of up to 24 in-lb. along the whole length, for test lengths up to three feet long (or even longer with slight modifications). Additional capability for simultaneously applying a torsion load of up to 3.6 in-lb. was provided. A platform was also constructed below the tip of the boom to measure the bending and twist deflections. This machine is shown in Figure 1.2.14. It was subsequently found that the bending strength was fairly uniform along the length, and that small torsion loads (under .1 in-lb.) and small shear loads (under 2 lb.) had no effect on the bending strength so that much of the testing for bending strength was done simply by an end-mass cantilever load.

The bending strengths have been determined experimentally and the average strengths are given below. Sufficient tests have not been made to give the 3σ deviation but it is approximately 10% for small values of A_w and 20% for large values.

A_w	Bending Strength (in-lb.)
0	14.5
.17	8.5
.33	5
.48	3

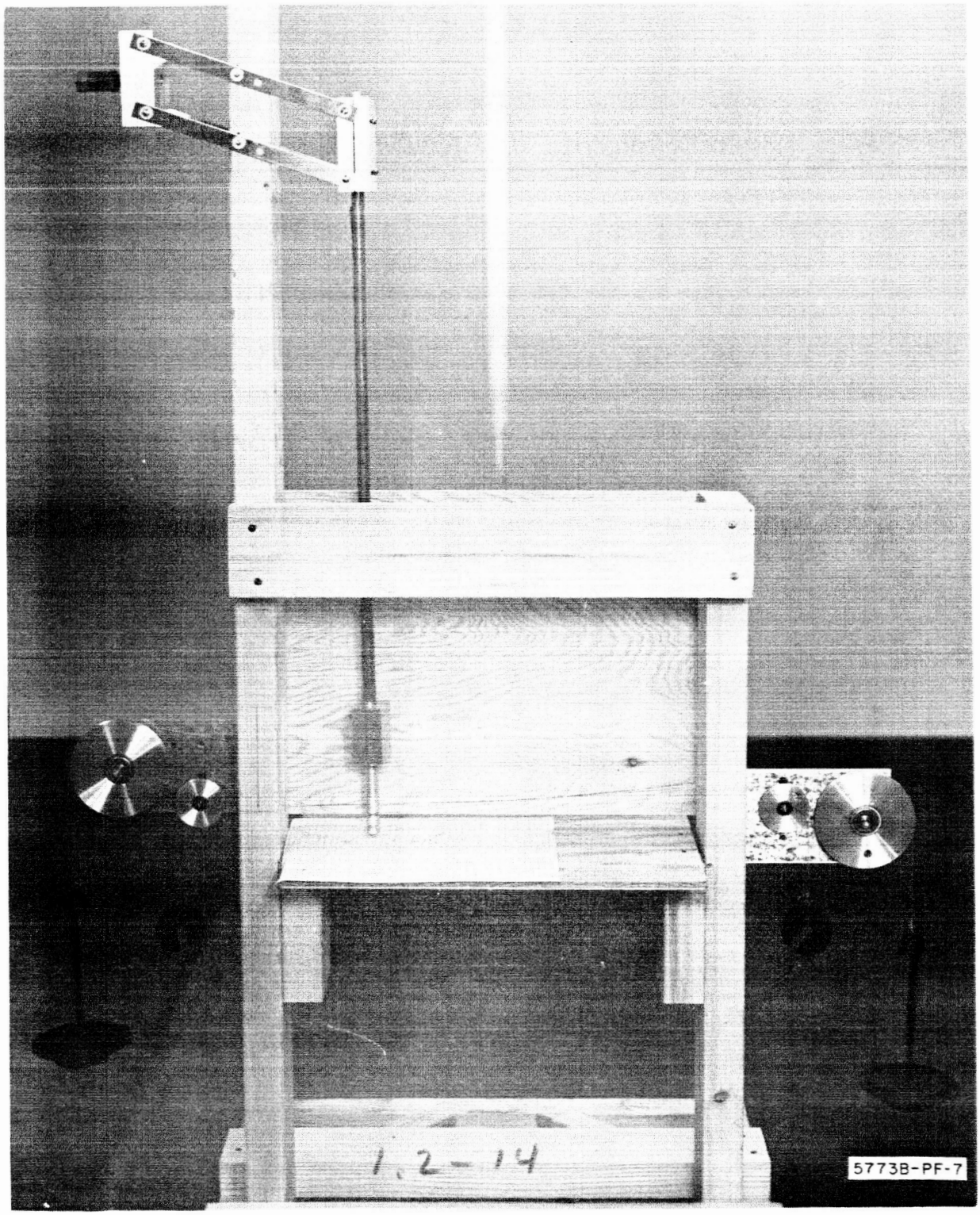

Figure 1.2.14 Bending Tester

The torsional strengths have also been determined experimentally. The strength is a function of the number of tabs per inch. Typical values are given below for the present tab design of 1 1/3 tabs per inch.

A_w	Torsional Strength (in-lb.)
0	1 +
.17	1 +
.33	1 +
.48	1 +

1.2.5 Mask Preparation

1.2.5.1 Drawings

In order to provide the film for the photo-etch process in making the window pattern in the boom, several preliminary steps are required. First, a sketch is made of the pattern giving all the dimensions. This is a sketch of a specific length of the boom in the flattened condition. It shows the tabs, notches and windows. The length of the sketch is some multiple of the distance between notches, usually from two to six times the notch pitch. This pattern is then made on a strip coat, a clear sheet of mylar with a red opaque coating. The pattern, a positive, is made by removing part of the coating by means of a mechanical drafting machine called a coordinatograph to a precision of about .001 inches. The pattern is usually made to a larger scale, up to ten-to-one, and then reduced to actual size on a strip of film. Any length of film can be exposed by a step-and-repeat process and the only alignment which must be held very accurately is the angular alignment, i.e., the edge of the pattern must form a straight line. To aid in this step-and-repeat alignment, a long guide line exactly parallel to the edge of the pattern is made on the strip coat. This process is perfectly suitable for booms up to 10 feet in length. For longer booms, a similar but improved process would be employed, but the process would remain unchanged up to the stage of the fabrication of the strip coat. Either a positive or negative is made from the film depending on the photo resist to be used in the etching process.

1.3 Material

1.3.1 Specification

Boom material is beryllium copper which has been procured from the Hamilton Watch Company to the following specification:

No. 25 alloy strip 2 ± 0.001 inch wide by 0.002 ± 0.00015 inches thick with the following characteristics:

(1) Solution treated, one-half hard, hardenable to 165,000 to 185,000 psi yield -- 0.2 percent offset.

(2) Grain size suitable to yield 3 grains per 0.002 inch thickness after aging.

(3) Maximum cross-bow vertical 0.125 inch.

(4) Longitudinal straightness maximum 0.75 inch out in 20 feet.

(5) Edge ripple maximum 0.10 inch with a 6 inch minimum period.

(6) Surface to be clean and free of oxides, marks and scratches.

(7) Chemical and physical properties to be supplied with each shipment.

1.3.2 Material Tests

Test specimens were heat treated to check the material over a range of time-temperature combinations. Tensile strength and spring back from elastic distortion were determined. Figure 1.3.1 shows a metal fixture which holds a tensile test specimen and a bent piece ready for heat treatment, and it also shows bent specimens after heat treatment. It is significant that some of the bent pieces came out of heat treatment with greater bends than determined by the fixtures. The permanent set increases with time at a given temperature and at the higher temperatures the bending started to reverse itself after a given time. This phenomenon was somewhat unexpected, but it has proven to be repeatable and has been used to advantage in making the booms.

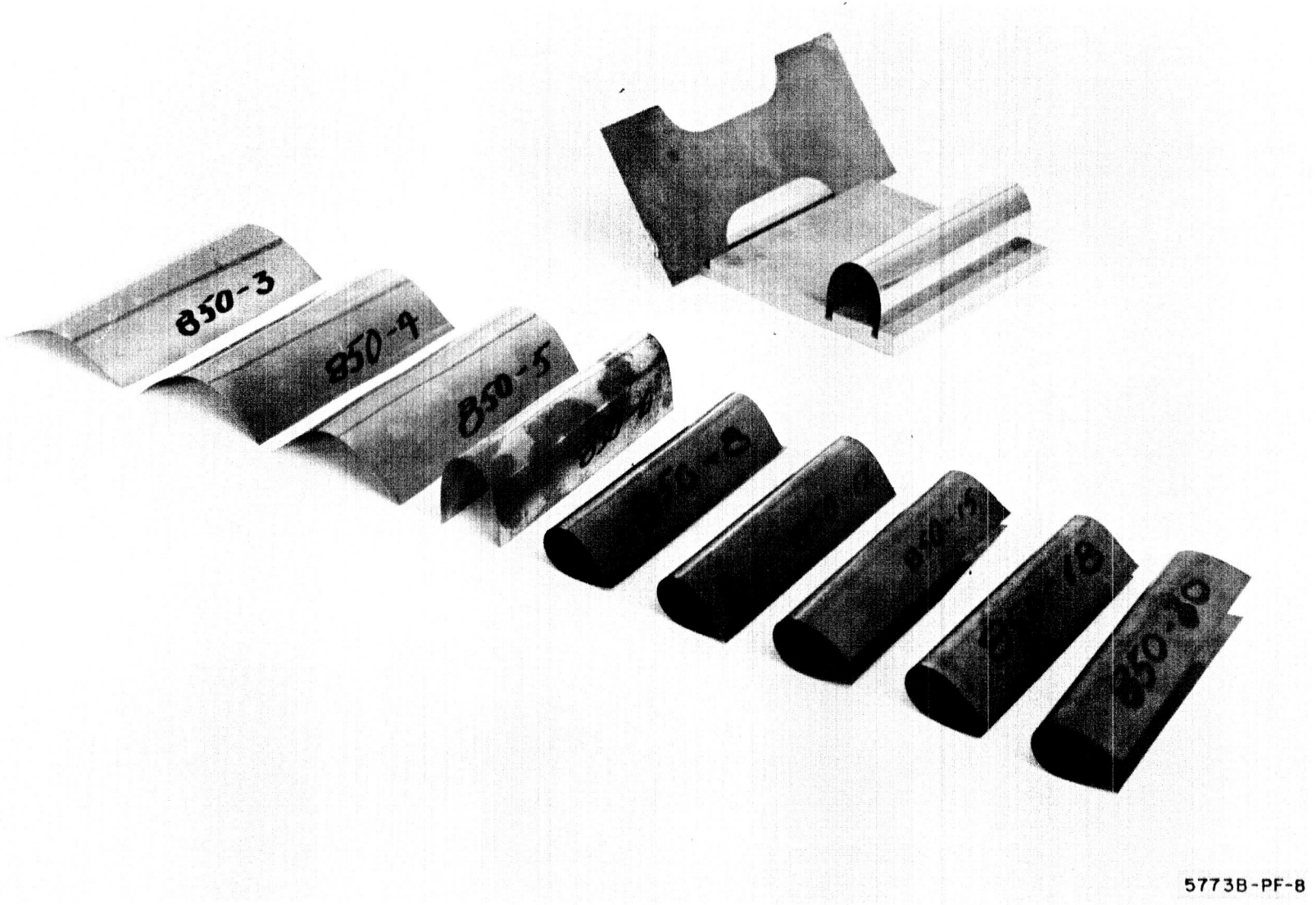

Figure 1.3.1 Beryllium Copper Specimens Before and After Heat Treatment

Temperatures used in this test were 600°, 800°, 825°, 850°, and 900°F and time was varied to reach the maximum ultimate strength. The ultimate strength fell between 170,000 and 180,000 psi. It was reached at the following times at the given temperatures: 180 minutes at 600°F, 12 minutes at 800°F, 10 minutes at 825°F, and 7 minutes at 900°F.

In the early stages of the project, some fully aged Brush Beryllium beryllium copper was tried. It was heat treated in the range from 700°F to 1000°F and the times were varied from 2 to 20 minutes. The bent test pieces took sets up to the complete amount determined by the fixture, but the bending did not extend beyond the fixture's limit as in the case of the unaged material from Hamilton. In all cases, the heat treatment degraded the strength characteristics.

1.3.3 Adaptation of Furnace to Material

With guidance from the above material tests, a large number of specimens were put through the furnace and then checked for shape and yield strength. Easily controlable and predictable conditions under which good booms could be made were determined and applied; however, good correlation with the earlier data has not been produced.

A simple means for checking yield in the material was applied in order to obtain prompt guidance from the trials. It is based on the fact that the bending stress in a beam is inversely proportional to the radius of curvature of the bend. For example, a 0.4 inch diameter, 0.002 inch thick, beryllium copper tube will be stressed up to 104,000 psi when flattened out. Additional stress is produced when it is further bent in reverse around a cylinder. For use in these trials a series of cylinders were made in the form of a stepped mandrel, Figure 1.3.2, such that the above specimen if bent backwards around the largest diameter step would be stressed up to 120,000 psi and then in steps of 10,000 psi to the top step which gives 160,000 psi.

In evaluating a test run, the unsprung diameters were measured and then 3/4 inch long sections of tubing were bent backward on the stepped

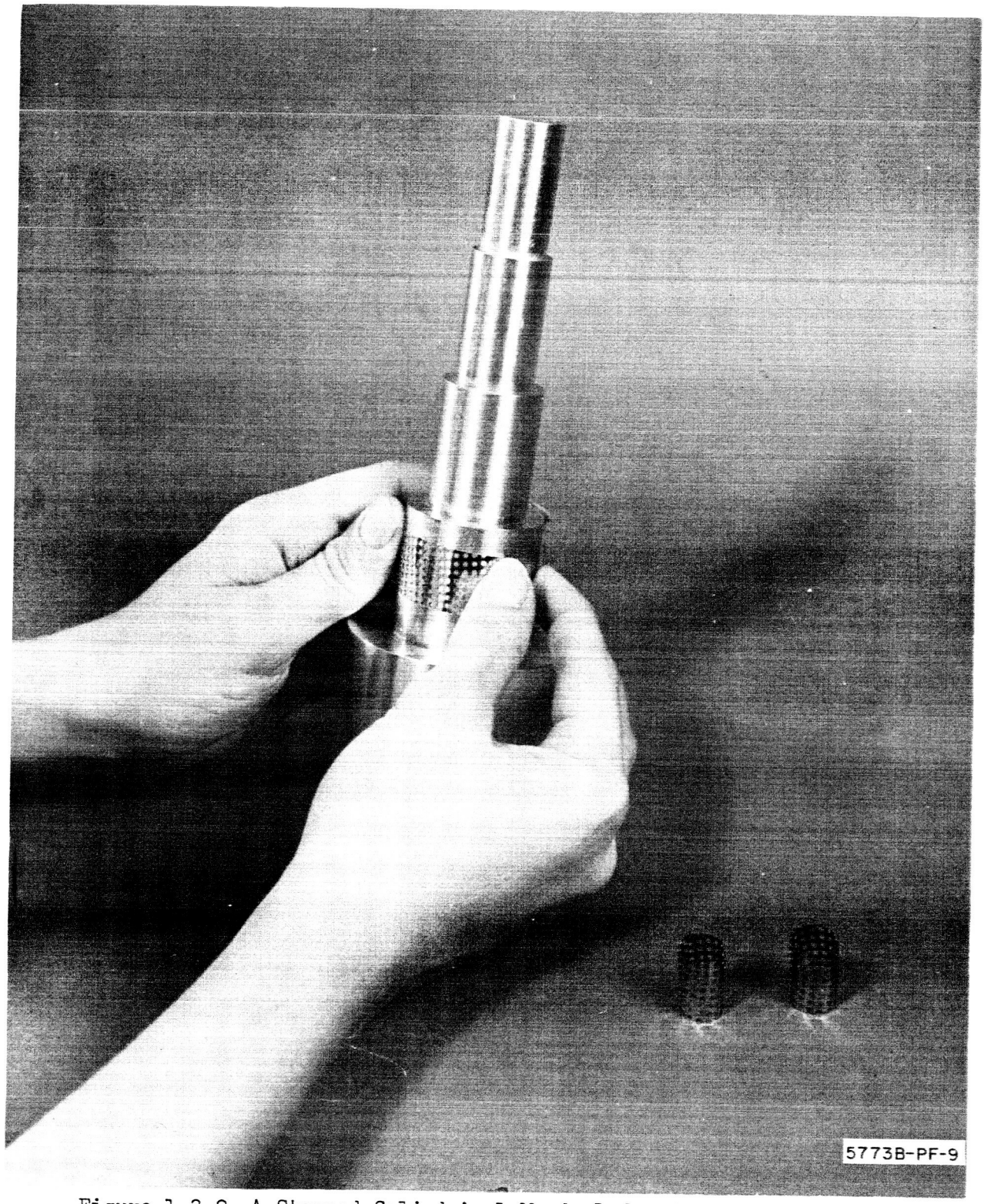

Figure 1.3.2 A Stepped Cylindrical Mandrel for Application of Known Amounts of Bending Stress to Trim Strips

cylinder. The cylinder diameter and the circumferential permanent set was noted for each step. Figure 1.3.3 shows the measurements made for a range of temperatures. It will be noted that over the entire range, the yield stress as determined by the change in radius of curvature is higher than the stress in the flattened tube. Verification through endurance runs of selected booms up to 100 cycles in a deployer have shown no signs of fatigue distress.

The treatment selected for the 10 foot lengths to be delivered is at 610°F.

1.4 Methods and Processes

1.4.1 Summary

All problem areas have been resolved and the continuous process, which was one of the stipulations of phase two, is in operation. The processes and developments acquired in this study contract are readily adaptable to a production mode of operation. There is little doubt that a pilot or production line could be assembled to successfully produce booms in the hundreds or thousands of feet.

1.4.2 Storage of Material

All material from which deliverable booms were to be made was stored in a vacuum until ready for use and exclusively handled with white gloves through the complete processing. Preliminary inspection of the material was always performed although it was usually in good shape. Such things as ripples, scratches, straightness, dirt, grease, and oxide are looked for and those faults which can be remedied are corrected.

1.4.3 Cleaning

A cleaning and drying procedure is standard and was found to be very necessary to remove oils which had accumulated on the material surface from the rolling mill operation. It involves a relatively simple dipping and drying operation. It consists of a dip in Shipley's Al-Chelate degreaser, a water bath and either a blot or oven dry. It could be easily automated.

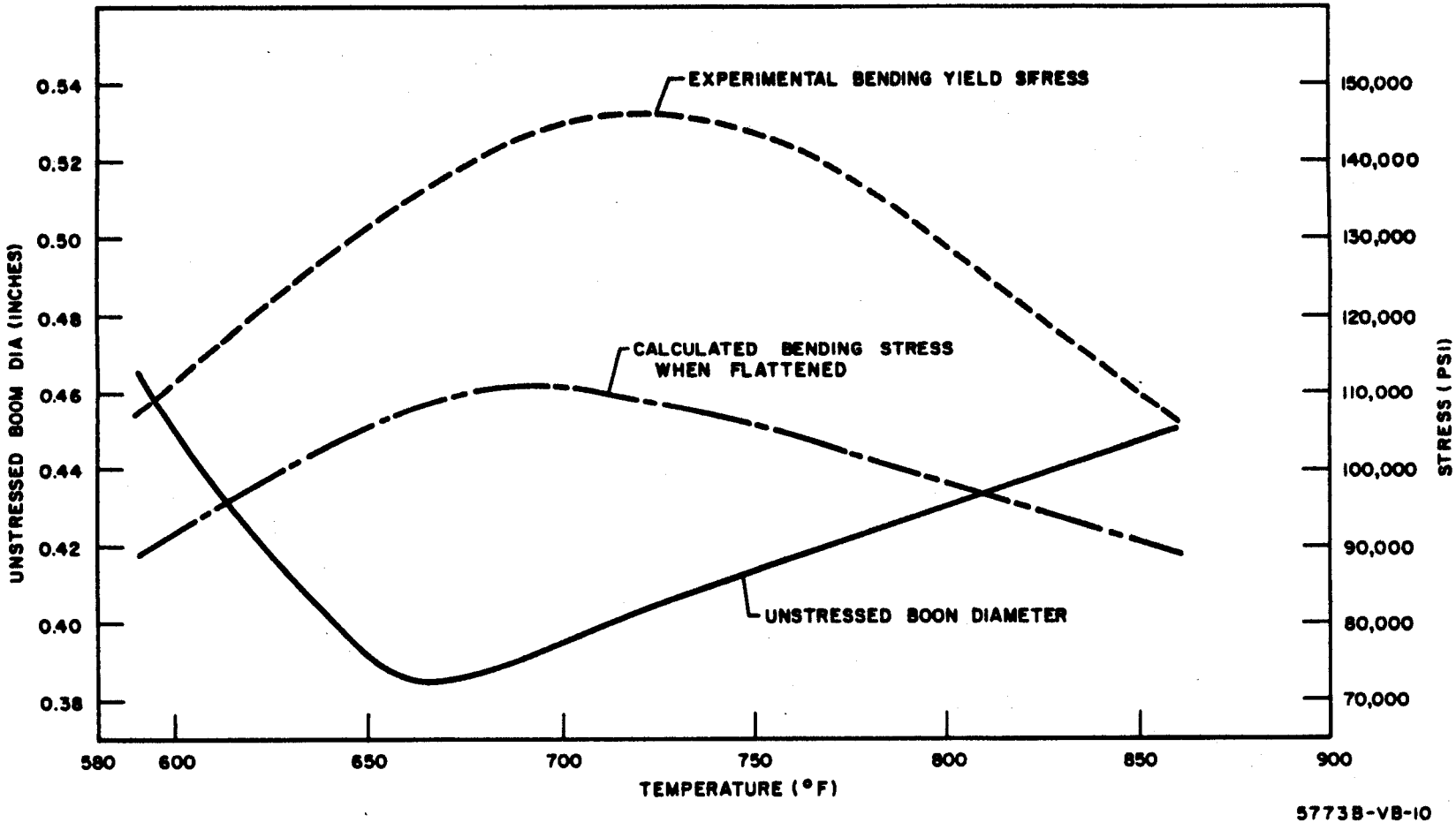

Figure 1.3.3 Tube Diameter and Stress vs Heat Treatment Temperature

1.4.4 Coating

Following cleaning, a coating of photo resist is applied to the complete surface of the material.

Various photo resists from different manufacturers were evaluated resulting in a product of Shipley Corp., called AZ-340, being selected. This produot proved much easier to expose and develop, and is entirely free from pin holes if the necessary precautions are taken. Pin holing was a major cause for concern in the early stages of the contract but the techniques developed and the discovery of AZ-340 completely eliminated this problem.

Dip coating has proven very satisfactory. It is a method whereby the material is placed in a container of photo resist and is pulled out at a constant rate, Figure 1.4.1. It was found that a rate of 10 in/min. was desirable and resulted in a smooth coat of uniform thickness. Hot air dryers could be installed to blow on the material after it emerges from the liquid; it would then be dry enough to go directly on rollers or a reel and would facilitate the processing of much longer strips.

Another method of applying the resist is by a roller coater which may also prove desirable for longer booms. This method is presently being worked on at Aerospace for coating printed circuit boards but has not been employed in this contract. Shipley has also been working in this area and has already proven its capability in the process.

Following coating, the material was dried in one of two ways, either by baking at 175°F for 25 min. or allowed to remain in clean room ambient for 16 hours. Both methods proved entirely satisfactory.

1.4.5 Mask Preparation

Various configurations of hole patterns and edge locking notches were considered and fabricated. These patterns were made into photographic masks by making an original layout greater than full size on a drafting table either by the use of black tape or ruby-lith. This was then reduced to the desired size by a photographic reducing technique

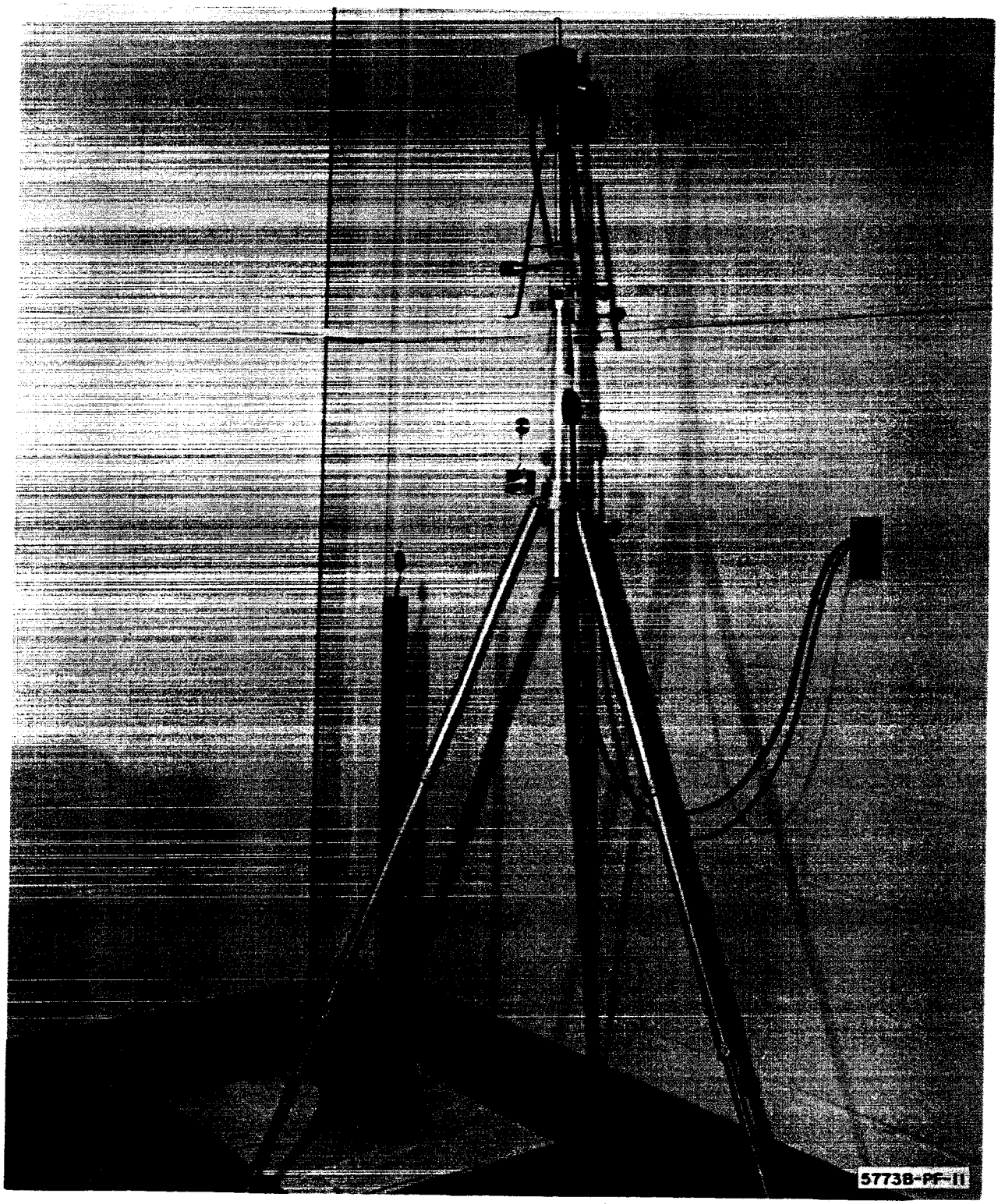

Figure 1.4.1 Application of Photo Resist

resulting in a negative of the correct dimensions. In the latter cases photographic step and repeat methods were used whereby a single negative pattern was repeated end to end resulting in a 42 inch positive film strip. The contact mask necessary for the chemical etching process is then produced, Figure 1.4.2.

1.4.6 Printing

The photo resist used was a positive photo resist sensitive to light in the ultraviolet wave length region. This means that it de-emulsified with impinging ultraviolet radiation. An exposure box was therefore used which incorporated a positive contact mask for printing the desired image, Figure 1.4.3. It consists of an upper and lower lamp housing 50 inches long and containing quick starter strips and 40 watt, "black light", ultraviolet fluorescent tubes. The lower housing supports two 1/2 inch thick plexi-glass sheets between which the copper strip and photo mask are sandwiched and supported. Steel bars are positioned on both sides of the mask assembly to act as weights, thus insuring intimate contact between the mask and the coated material. Opaque film and clamps are affixed at both ends of the exposure assembly and registration is accomplished so as to make feasible a continuous step and repeat operation for lengths greater than 40 inches. Light-tight ports are contained in each end of the enclosure assembly and allow photo sensitive copper to protrude from both ends while its center is being exposed to the desired pattern. Each housing has its own switch which enables exposure from one side only or exposure of different periods on each side.

This operation is easily convertible into a continuous process, by stepping and registering the mask along the length of the boom. It could be even more automated with the photo sensitive material paying off a storage reel onto a drum where the desired hole pattern would move with the material as it is subjected to exposure. It would then run directly into the developing tank for the final photographic processing.

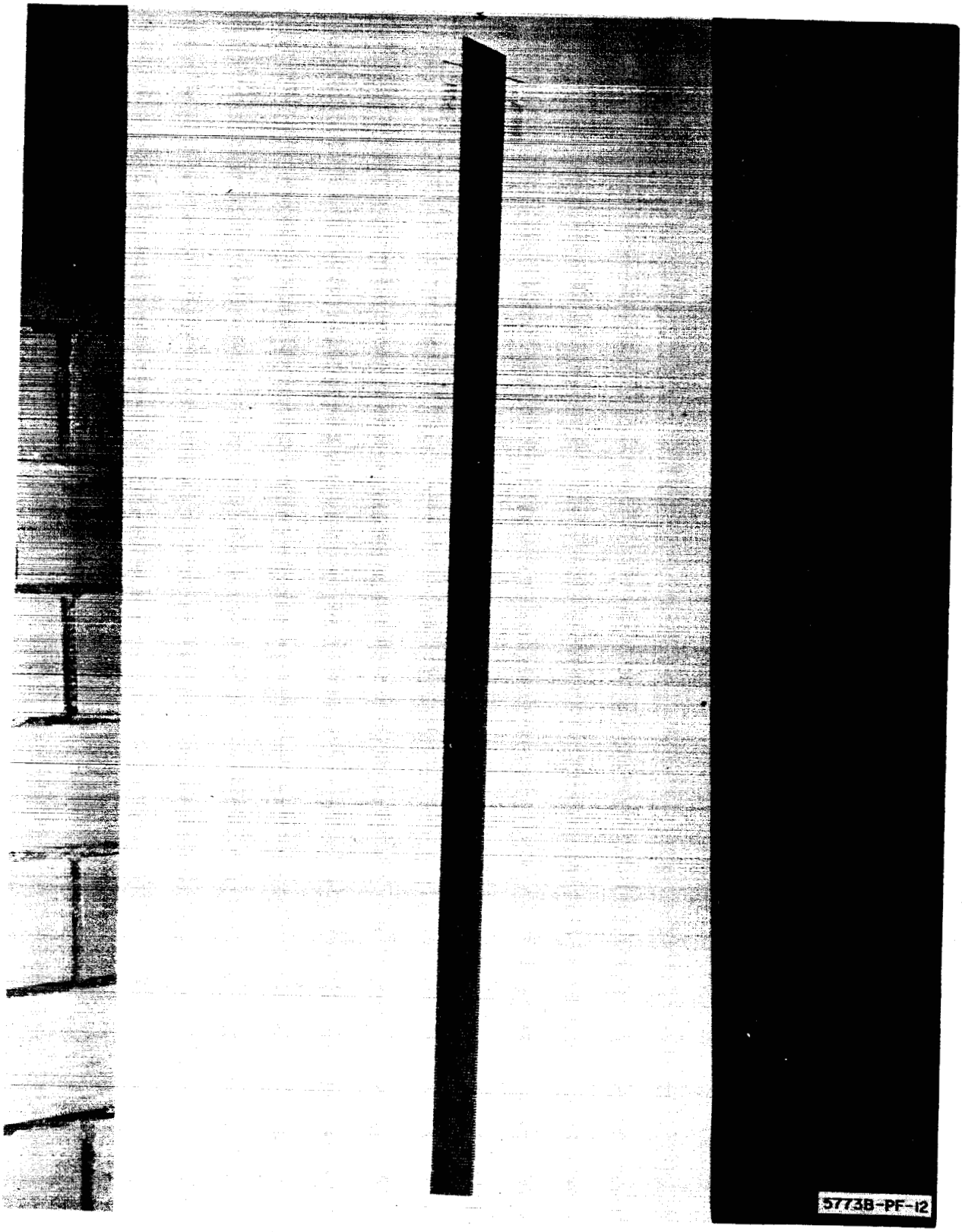

Figure 1.4.2 Photographic Mask

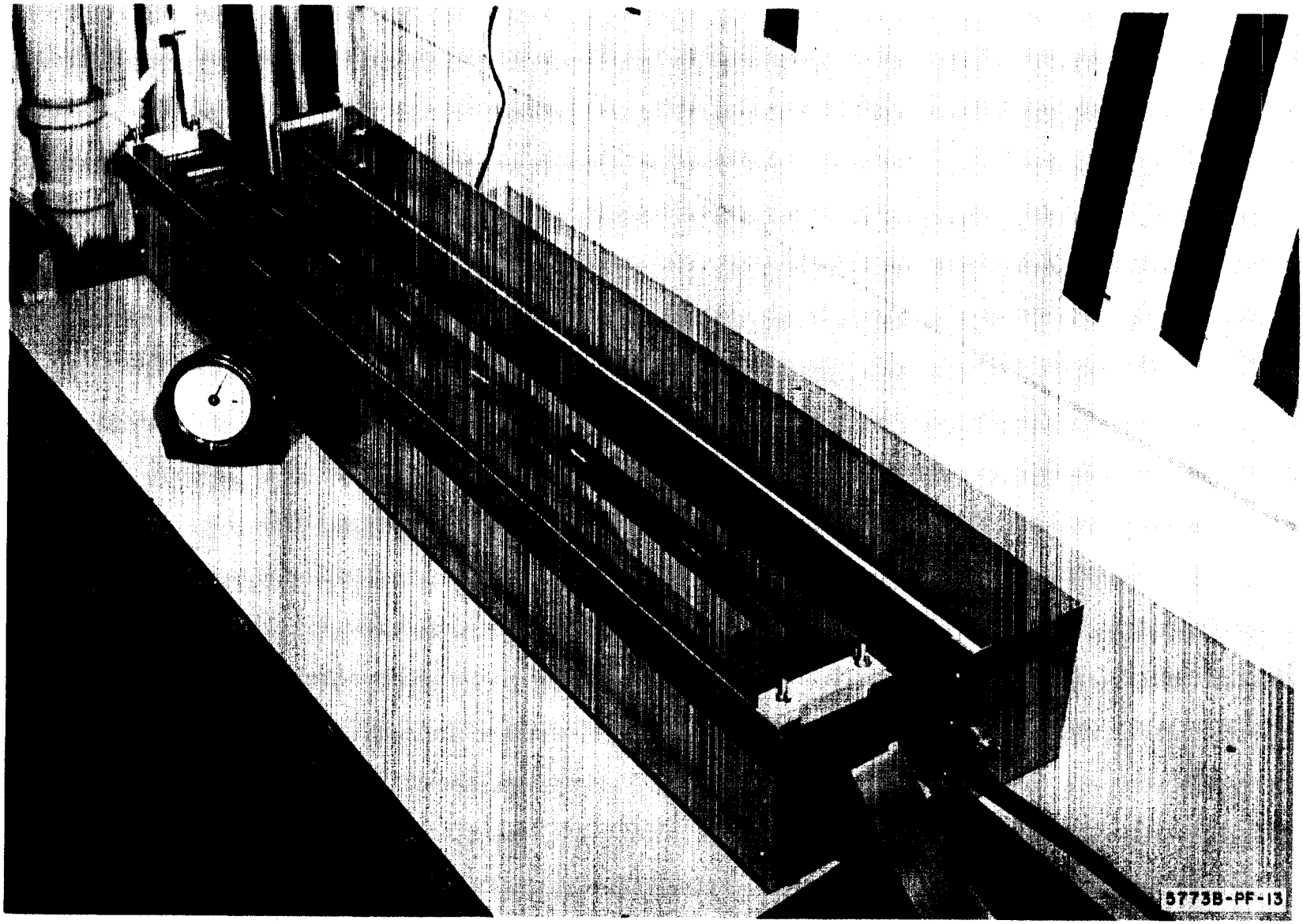

Figure 1.4.3 Exposure Box

1.4.7 Developing

Developing has been satisfactorily accomplished with the most rudimentary equipment, Figure 1.4.4. The process is not overly critical and was performed quite readily by two operators. The material is deployed from a supply pully system into a developer tray containing AZ-300 developer. It then proceeds to a fine water spray and submersion to stop the developing process as well as help remove the developed photo resist. From this point it progresses to the drying area where it is blotted dry with absorbent towels and finally to a take up pulley system from which it is stored until ready for chemical milling.

1.4.8 Chemical Milling

The chemical milling was performed in a Chemicut Spray Etcher, Model 502, which has oscillating sprays operating from both top and bottom, Figure 1.4.5. The material with its acid resistant pattern is transported through the chromic sulfuric acid spray by means of a conveyor system which moves the sample at a uniform rate of 20 inches per minute and emerges from the other side completely milled to desired specifications. If both sides of the strip have the pattern in the photo-resist then both the top and bottom spray is used, but if the pattern is on the top only then the corresponding top spray is used. It was found that one sided etching was sufficient and eliminated the tedious registration problem of a double sided mask.

The equipment very closely approximates the apparatus which would be expected in a production line assembly. The physical size and appearance would no doubt change but the overall operation would remain the same.

1.4.9 Final Cleaning

The etched material was then subjected to a chemical bath and water rinse sequence much like the developing procedure. This time the chemical was a Shipley product called Al-Chelate which easily removed

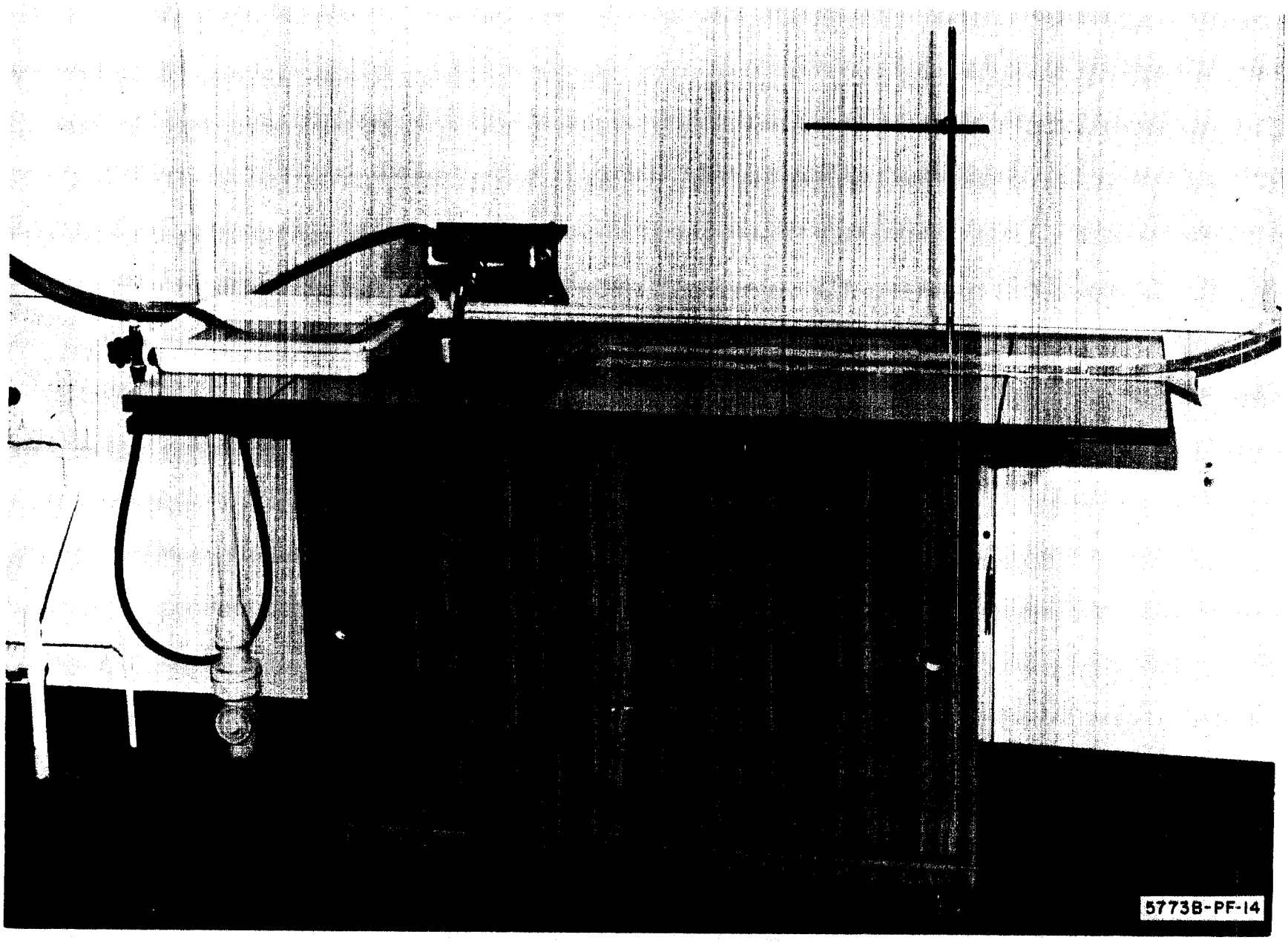

Figure 1.4.4 Developer

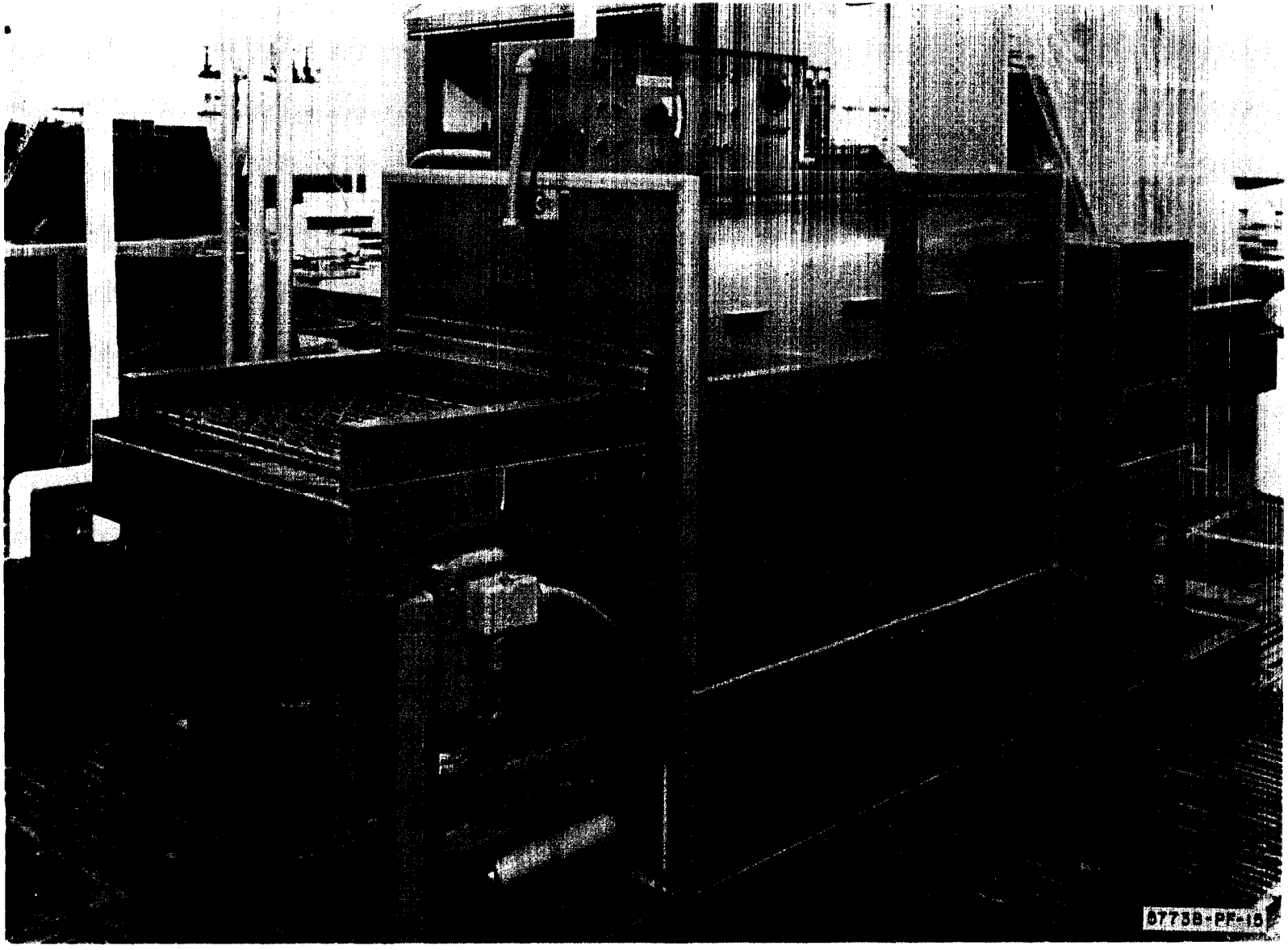

Figure 1.4.5 Etcher

the remaining photo resist. Unlike the developing procedure the material is given a quick dip in ammonium persulfate to remove any oxide which may be on its surface prior to the rinse and drying process. Both the processes could be simply performed by a series of rollers and chemical submersion baths, plus water spray and submersion baths.

1.4.10 Tab Forming

Alternate tabs are now preset by a unique tab bending apparatus, Figure 1.4.6. This operation was performed on both edges of the etched material prior to the forming and heat treating. It was operated by a single operator who propelled the material laterally through the bending jaws as he applied the deformation force with a foot treadle. A similar apparatus could be automated which would step the material through a registration device and preset the tabs with a solenoid. It is more probable that some sort of rolling device would be designed to preset both edges simultaneously as the material moved smoothly through its die forms.

1.4.11 Heat Treatment

Two basically different ovens were designed and built corresponding to the two phases of the contract. The first was a 50 inch oven capable of processing the 3 foot booms required in phase one. It consisted of 10 individually controllable heater elements spiraled in a continuous manner about a 1 inch steel supporting pipe. Covering the heater elements was 1 inch of asbestos and covering the asbestos was 1 inch of magnesia. This assembly was supported on a sturdy wooden base and was controlled by a master 45 amp single phase power stat, Figure 1.4.7. The heater elements are Glas-Col capable of 1112 degrees F. and a power dissipation of 500 watts each. The elements may be adjusted to give a uniform thermal profile and the end of the supporting pipe was capped with a nipple to allow a flow of Argon gas to prevent oxidation of the copper. A 50 inch cooling tube was placed on the front of the oven so that the boom could be pulled directly from the hot zone into a cool Argon atmosphere without being subjected to oxidation.

Figure 1.4.6 Tab Bender

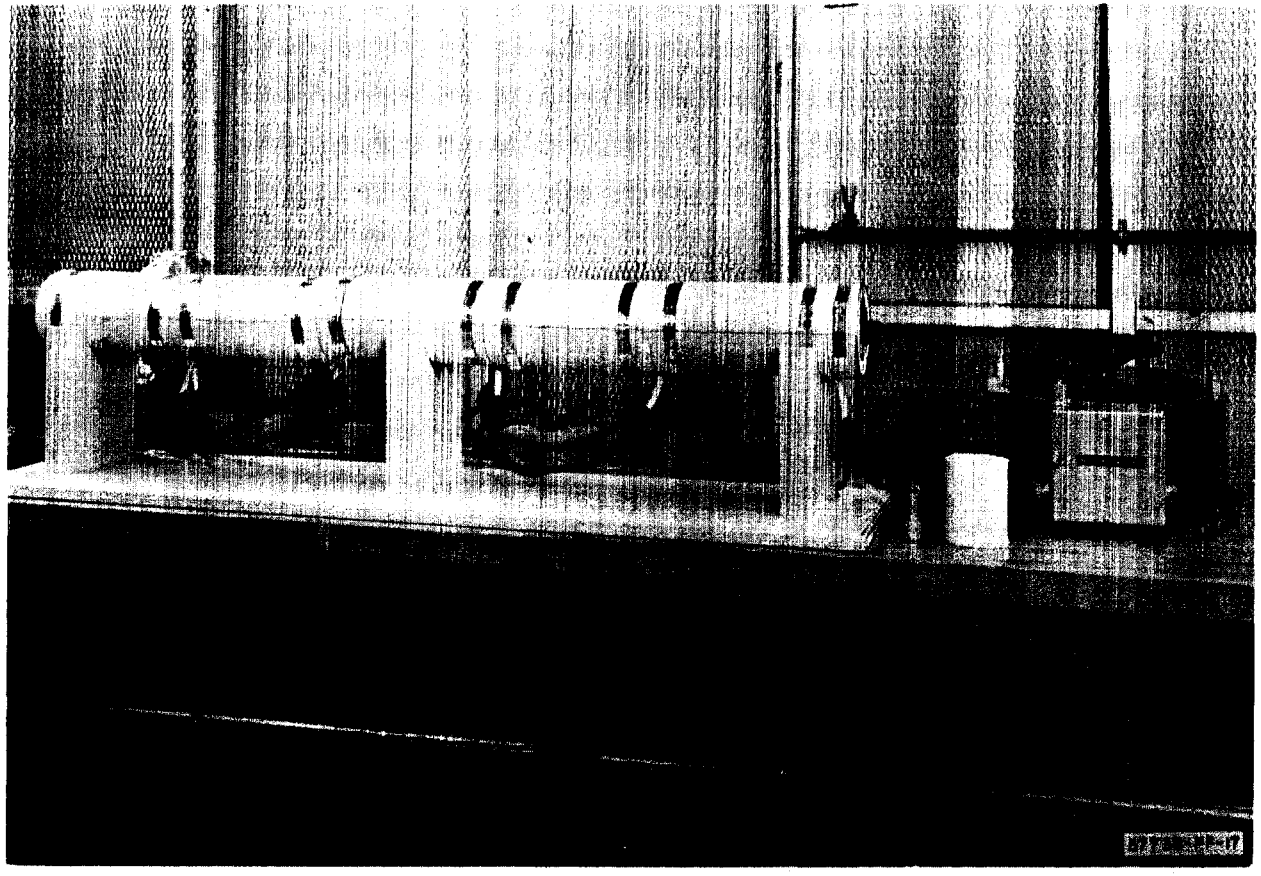

Figure 1.4.7 Heat Treater and Former

A 42 inch piece of etched material was first pulled into a 1/2 inch diameter copper tube by using a series of funnels and a special pulling clamp. It was then inserted into the cooling tube and purged of all air by flushing it with a flow of Argon. At this point it was pushed into the hot zone of the oven and allowed to remain for the predetermined time. Following this heat treat it then was pulled back into the cooling tube and allowed to cool to room temperature. After removal from the cooling tube the tabs were alternately bent and the boom zippered and placed in the vacuum shipping tube.

The most troublesome segments of this operation were: - inserting the material into the 1/2 inch diameter tube without crinkling it and finding the correct temperature to give the proper curl and strength; as well as keeping the oven profile uniform so that the boom would be of a uniform cross section throughout its length. These problems were rectified and booms of high quality were produced to satisfy phase one.

The second oven was designed and built for phase two which stipulated a continuous process of manufacture. This oven was designed and built four separate times in the effort to attain the ultimate in effective temperature and pulling attitude.

Techniques for constant pulling force and constant pulling rate were incorporated with the latter proving the most desirable. It was found that the curling property was too localized to affect the material prior to coming into the hot zone and it therefore had to be pulled in at a constant rate.

The final design consisted of a 27 inch oven, 2 pyrometer controlled power stats, a 14 ft. cooling tube, and a one rpm pulling motor. The first 7 inches of the oven contains two stainless steel forming funnels which are distinctively shaped to insure the material's attaining the correct configuration as it enters the final heat forming tube. The last 20 inches contains the final heat forming tube, which is also of stainless steel, and has a constant diameter of .506 inches. Glas-Col heater elements are used for heat generation as they were in

the phase one oven. Three thermocouples are precisely positioned along the length of the oven and their temperature is constantly monitored. The complete assembly was then wrapped with 2 inches of fiber glass insulation and securely fastened to a sturdy wooden base, Figure 1.4.8.

Twelve feet of material, with its tabs preformed, is placed on a spool, one end of which is attached to a pulling clamp. This clamp is fastened to a steel wire which runs through the oven and cooling tube and is secured to the pulling motor, Figure 1.4.9. As the motor pulls the material through the oven , at 2 inches per minute, it automatically engages its tabs and emerges as a completed boom, ready for shipment, Figure 1.4.10.

Pulling attitude and temperature were found to be critical. If the attitude was not correct the booms would emerge bent, and if the temperature were incorrect the curl and strength were poor. It is felt that the dependence of straightness on attitude may be an advantage in straightening bent booms or pulling straight booms from crooked material.

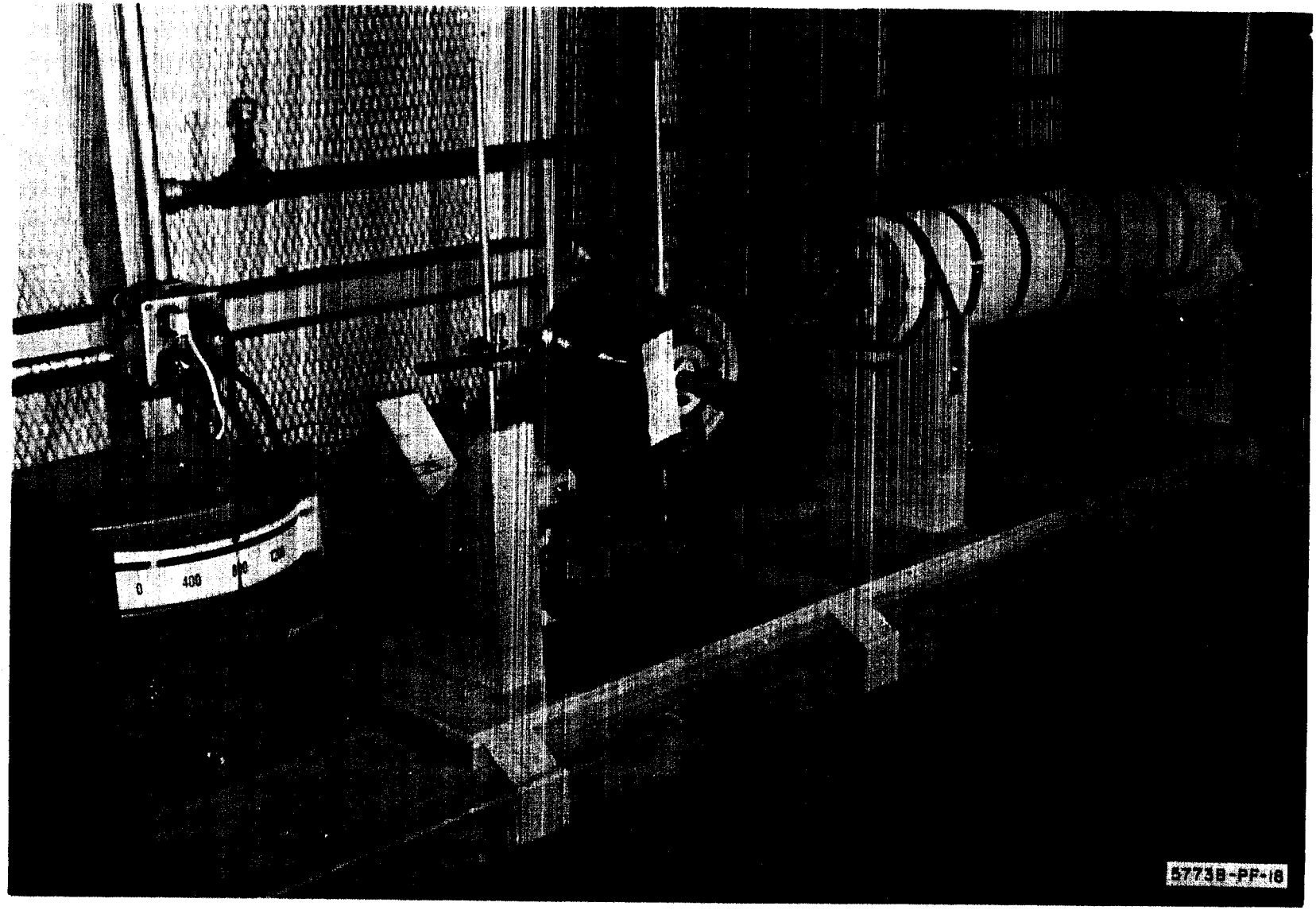

Figure 1.4.8 Continuous Heat Treater and Former

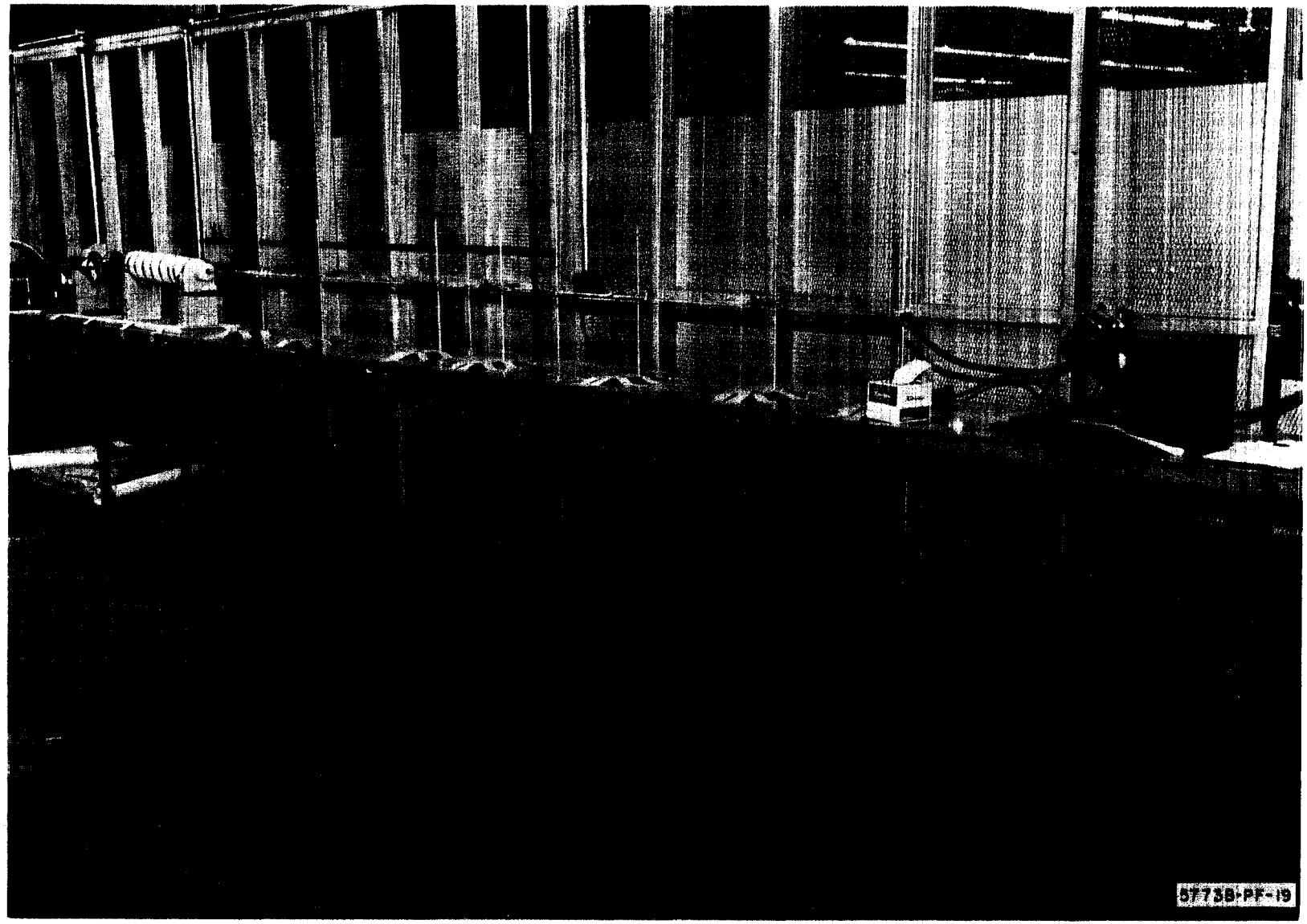

Figure 1.4.9 Heat Treatment

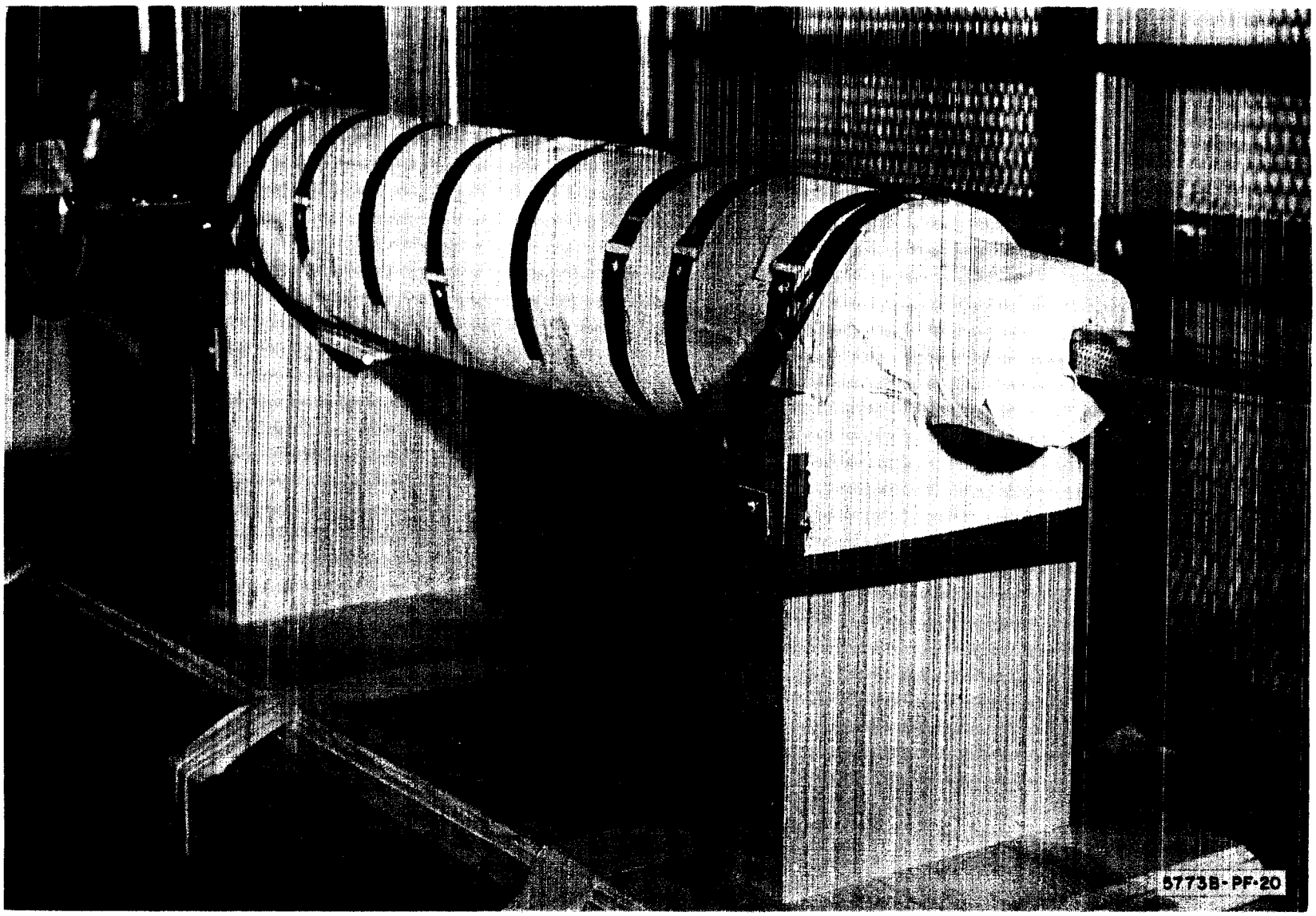

Figure 1.4.10 Boom Emerging from Heat Treatment

1.5 Deployer

1.5.1 Introduction

An engineering model of a mechanism for storing, deploying and retracting the extendable boom has been completed and tested. Figures 1.5.1 and 1.5.2 show two views of the deployer loaded with a boom. For convenience in testing and demonstrating a handle and a switch are attached.

1.5.2 Description of Design and Operation

The deployer is made up essentially of a storage drum, pinch rolls, a guide for deployment, and a means for driving. An important feature of the deployer is its use of two motors, one for deployment of the boom and the other for retraction. Preliminary design of a mechanism requiring only one motor was investigated on the drawing board, but a few significant conclusions quickly led to the adoption of the two motor approach. Underlying these conclusions was the necessary complexity involved in overrunning clutches to allow the two-way operation of the drive. The attendant number of parts and the indicated extensive development militated against the one-motor design.

In order to minimize the size and weight disadvantage inherent in the two-motor approach, the motors were placed within two of the cylindrical members which function as primary elements in the deploying mechanism. The dark colored ends of the two motors can be observed in Figure 1.5.1.

The deploying or extending motor location is the one closer to the end of the mechanism carrying the long guide extension. This end is called the front. A pinion on the motor shaft extending through a clearance hole in the left side of the frame engages a gear on the power roller. The location of the power roller is above the front motor in Figure 1.5.1.

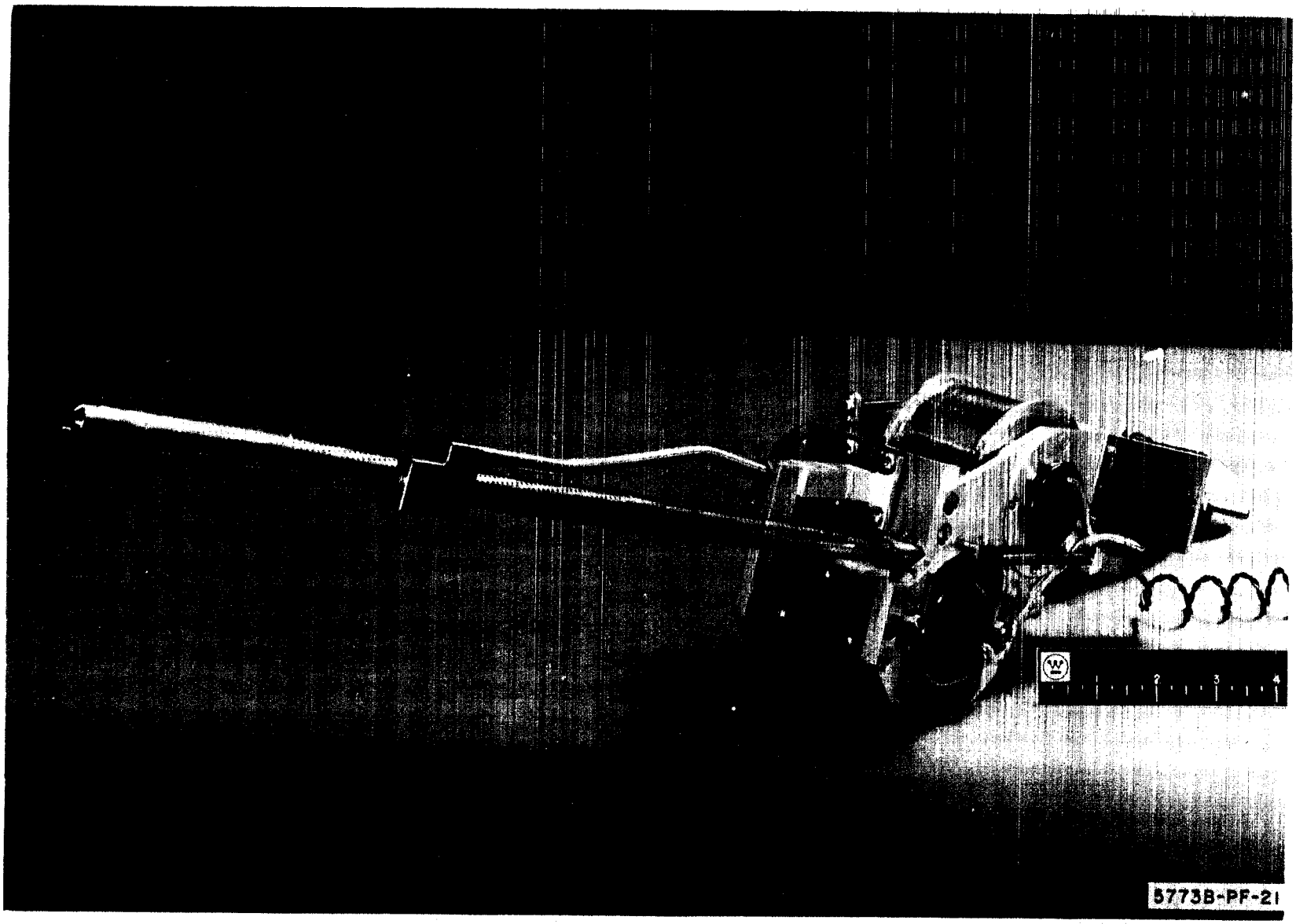

Figure 1.5.1 Deployer - Front View

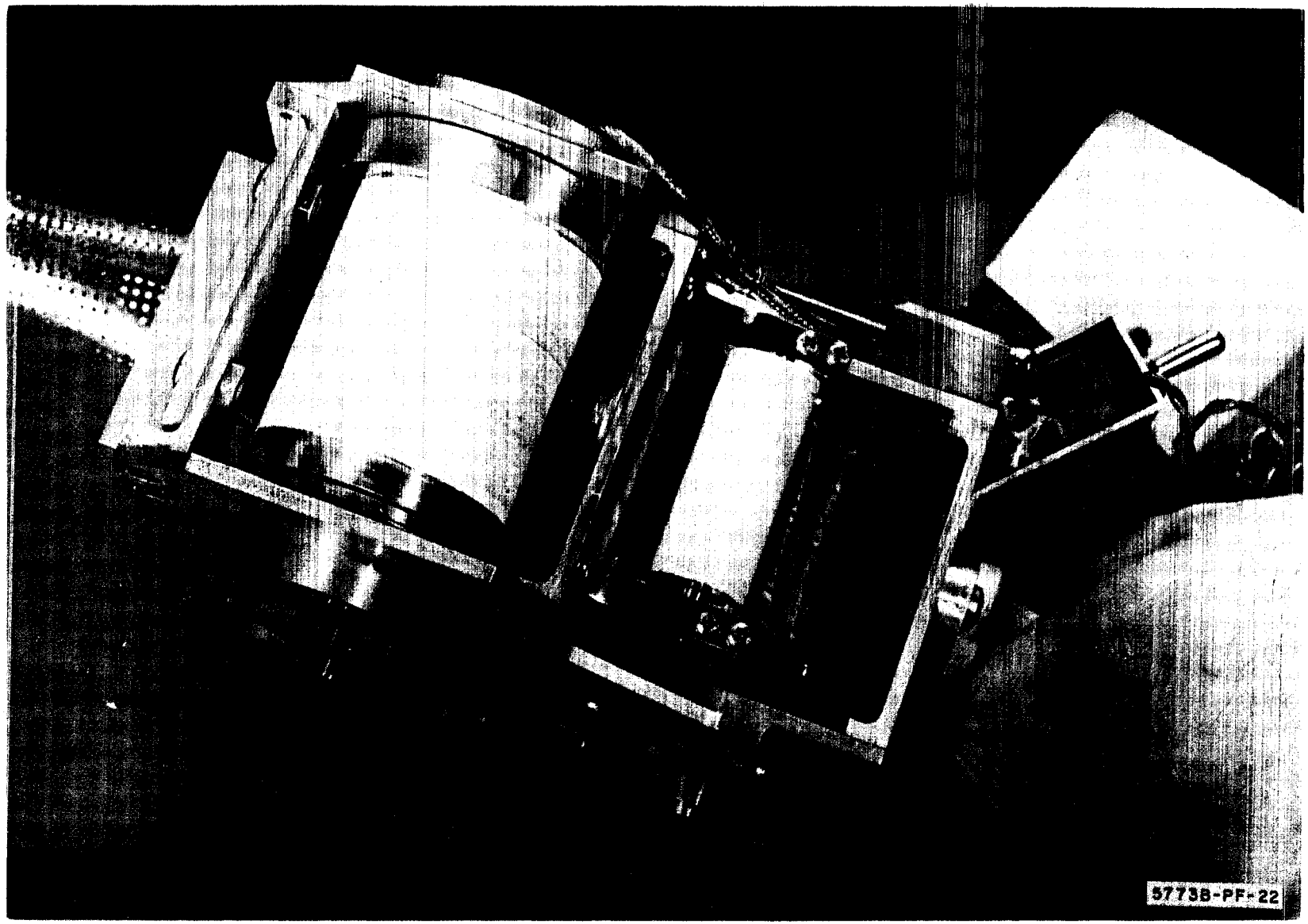

Figure 1.5.2 Deployer - Bottom View

The flat boom is driven out by the power roller much as clothes are pulled through the wringer of the older style washing machine. The undriven pressure roller surrounds the motor and is spring loaded against the power roller by the cantilever spring rods which are mounted at the rear of the frame and extend forward. Both the power roller and the undriven pressure roller are surfaced with a high-friction silicone rubber which has been space approved for the Gemini project. The rubber provides the necessary driving friction and also protects the boom material from scratches and similar abuse.

The retracting motor is located toward the back as seen in Figure 1.5.1. Again, a motor shaft extends through the left frame wall and carries a pinion which engages an intermediate gear. This intermediate gear in turn drives a ring gear cut on an internal rim of the reel. The flattened boom material is wound on the reel.

To prevent the elastic properties of the boom material from partially coiling on the reel and ultimately upsetting deployer operation, a drag roller with adjustable friction torque is caused to bear against the reel, Figure 1.5.2. The result is that tension is always maintained in the boom material and it is kept tightly wound on the reel. A refinement of this drag mechanism will probably be required to insure satisfactory maintenance of tension in the coiled, stored material on the reel during vibration. In any event, no undesired deployment of the boom past the power roller would occur even if looseness were to develop in the stored material.

A guide shoe is used to ease the transition of the material of the boom from the flat to the tubular condition, or the converse depending upon the mode of operation.

The boom guide at the front end of the assembly has as its major purpose the provision of bending moment reaction for the extended boom. In addition, it is an alignment device to maintain straight reeling and unreeling of the boom.

A zippering aid is located in the partially coiled boom between the shoe and guide. It is a male, tapered mandrel supported on a small rod seen in Figure 1.5.1. It lies within the forming boom just behind the boom guide and bears a slight valley or depression on the upper side running lengthwise with the boom. As the boom edges come together in the forming boom, the inward bent zippering tabs are allowed to bend down into the valley while the unbent tabs are held upward by the surface of the mandrel just behind the tabs. The result is an exaggeration of the height difference between opposing tabs and an increased reliability in the zippering action.

1.5.3 Size and Weight

The weight of the deployer with the handle and switch as shown in Figure 1.5.1 is 4.6 pounds. Included are the weights of the motors at 8.5 oz. each. The volume of a parallelepiped which fully contains the deployer approximates 0.23 cubic feet. Considerable weight savings can be realized in a refined design although not much size reduction is anticipated. Both weight and size estimates are based upon capacity for a 100 foot boom, the length for which the illustrated deployer has been designed. Longer boom lengths will necessitate larger frame clearance and the like.

1.5.4 Material and Component Considerations for Space

Material considerations have not been ignored during deployer design. Nevertheless, in the interest of rapid parts procurement and fabrication, material requirements have been subordinated, knowingly. Perhaps the chief concern in this respect is the bearing lubrication problem. The design calls for the use of ball bearings on all rollers and reels. Such bearings are especially necessary on the reel and the undriven pressure roller inasmuch as these items have large open bores to contain the drive motors. Consequently, friction radii are large.

Westinghouse, as well as other manufacturers, has developed sintered materials with various dry lubricant inclusions such as tungsten diselenide. Material of this type has been used in bearing retainers to provide a ball bearing operable in space. This kind of technology will have to be applied to the bearings and the gears of the flight deployer.

The drive motors also pose a problem for the flight unit. One avenue of solution would involve the use of a brushless motor such as the Sperry Farragut 9821 developed for G.S.F.C. It is doubtful that the 2 feet per second deployment rate could be sustained with this motor, however. Another approach could involve a sealed motor chamber with an elastic metal torque transmission to the outside. The United Shoe Harmonic Drive might be adapted to this application. A third possibility would lie in the direction of materials development for sliding electrical contacts useable in space. The Westinghouse Research Laboratories has been experiencing some success with Niobium diselenide for sliding electrical contacts in hard vacuum.

1.5.5 Test Results

A number of booms varying in length from 3 feet to 10 feet have been subjected to deployment and retraction. At the outset of testing it because apparent that certain heat treat cycles favored deployment more than others; but by refinement of the deployer shoe geometry and the addition of a control roller and the zippering guide the booms produced by nearly all practical heat treat cycles have been rendered capable of repeated deployment and retraction.

Two booms have been subjected to in excess of 100 cycles. A number have passed 40 cycles. One test specimen has been subjected to two tests of 5 cycles each separated by a one-week interval. During the interval the boom was stored in coiled form on a storage reel.

On the basis of observation during tests, it has been concluded that the booms as produced at this stage are entirely capable of at least 100 deployment and retraction cycles without evident damage to the tabs or the material. This indicates that stresses imposed during deployment, retraction and storage are safely below the yield strength and fatigue limit of the material.

APPENDIX I

EFFECT OF LENGTHWISE VARIATION IN IRRADIATION

The radiation on the far side of the boom has a variation along the length as noted in Section 1.2.2.2 and as seen in Figure 1.2.4. This variation causes a corresponding temperature variation. As long as this temperature variation ΔT is small (say 5°F) compared to the average temperature, T_m, the average emitted radiation from this surface will be equal to the radiation at the average temperature (i.e., $\Delta E = e \sigma (T^4 - T_m^4) \simeq e\sigma T_m^3 \Delta T$ if $\Delta T/T_m \ll 1$ where ΔE is the change in emitted radiation from the average, $T_m = \frac{T_{max} + T_{min}}{2}$, and $\Delta T = T - T_m$). This fact of ΔT being small then justifies assumption number 2 of Section 1.2.2.3. From Figure 1.2.4, it can be seen that the pattern of irradiation of the back surface is dependent on A_w. For the 17% hole pattern (second from left), a reasonable representation of the irradiation is:

Maximum irradiation = $A_w J_s$ (corresponding to black band in photo)

Average irradiation = $A_w J_s (1 - A_w)$

Minimum irradiation = $A_w J_s (1 - 2 A_w)$

Assuming a sinusoidal variation with a wave length of 3/8 inch, the irradiation of the far surface is given by:

$$J = A_w J_s (1 - A_w) + A_w^2 J_s \sin \frac{2\pi Z}{3/8}$$

as shown in Figure A-1.

$$J = A_w (1 - A_w) J_s + A_w^2 J_s \sin 16.7 Z$$

$$J_{AV} = A_{w_2} (1 - A_w) J_s$$

$$(J - J_{AV}) = A_w^2 J_s \sin 16.7 Z$$

(See Figure I-1)

The heat flow q along the length (in the Z direction) is given by:

$$q = \int (J - J_{AV}) \alpha_i D \, dZ$$

The root of the heat absorbed, $J_{AV} \alpha_i D \, dZ$, is dissipated by radiation

$$q = \alpha_i D A_w^2 J_s \int \sin 16.7 Z \, dZ$$

$$q = \frac{-\alpha_i D}{16.7} A_w^2 J_s \cos 16.7 Z + C_1$$

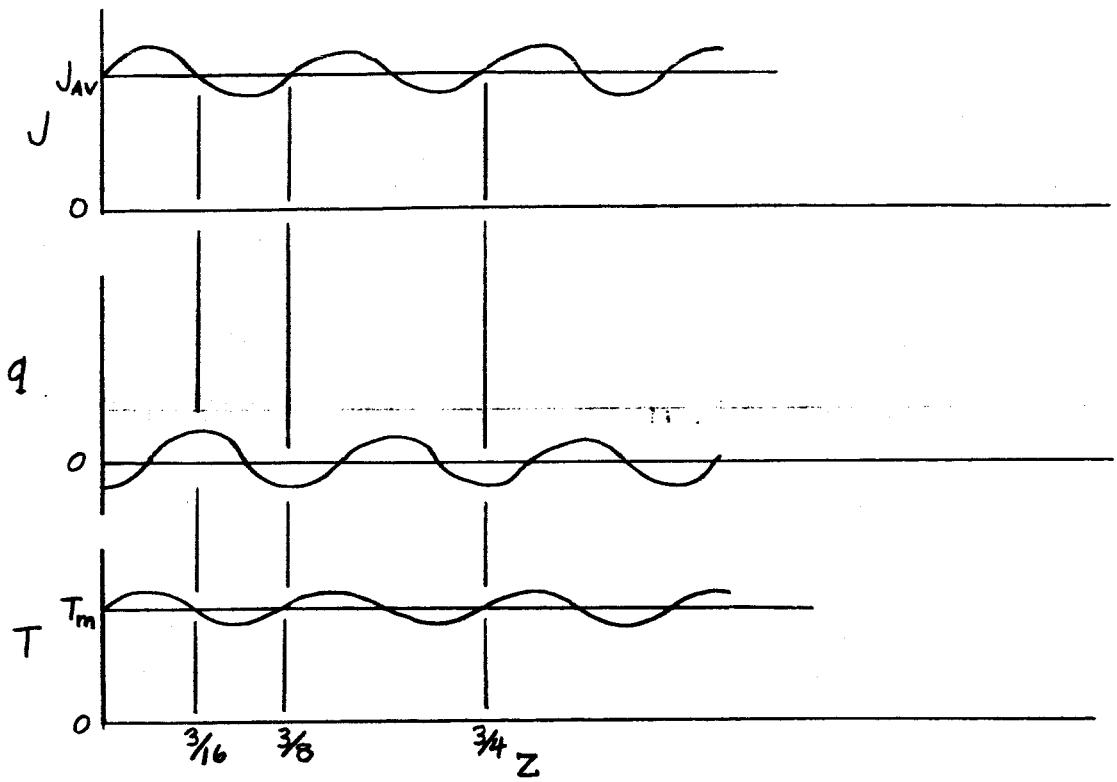

Figure I-1 Variation of J, q and T With Length

By symmetry, q = 0 at Z = 3/32

$\therefore C_1 = 0$

$$q = -k^1 A \frac{dT}{dZ}$$

$$q = -k^1 \pi/2 \, Dt \frac{dT}{dZ}$$

$$\frac{dT}{dZ} = \frac{2}{k^1 \pi \, Dt} \left(\frac{\alpha_i \, D}{16.7}\right) A_w^2 \, J_s \cos 16.7 \, Z$$

$$T = \frac{2}{k^1 \pi \, Dt} \frac{\alpha_i \, D}{16.7^2} A_w^2 \, J_s \sin 16.7 \, Z + C_2$$

Obviously $T = T_m$ at $Z = 0$.

The greatest temperature variation from the mean is therefore

$$(T - T_m)_{max} = \frac{2 \, \alpha_i \, A_w^2 \, J_s}{k^1 \pi \, t \, (16.7)^2}$$

Assuming $\alpha_i = 1.00$

$J_s = 3.12$ Btu/hr in^2

$k^1 = 2.72$ Btu/hr in°F

$t = .002$ in.

$A_w = .17$

$$\Delta T = (T - T_m)_{max} = \frac{2\,(1)\,(.17)^2\,(3.12)}{2.72\,(\pi)\,(.002)\,(16.7)^2}$$

$$\Delta T = (T - T_m)_{max} = .38°F$$

This is very small, and thus the analysis of Appendix B based on an average temperature is not invalidated by the variation of temperature in the axial direction.

APPENDIX II

To determine the thermal bending of a boom due to sunlight, it is necessary to write a heat balance equation for an element. It is assumed that there is no temperature gradient along the length of the boom. It is also assumed that $\Delta T/T << 1$ so that the heat radiated from every element is the same.

The heat balance for the element can be expressed as (See Figure II-1):

heat going in = heat going out

$$q_s + q_c = q_r + q_c + \frac{dq_c}{dx} dx$$

$$-\frac{dq_c}{dx} dx = q_r - q_s$$

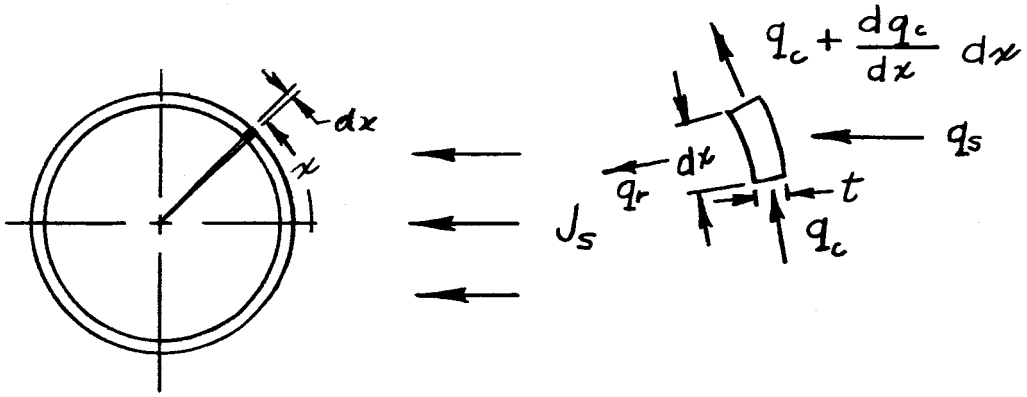

Figure II-1 Heat Flow For Elemental Strip

where

q_r = heat radiated from element

q_s = radiant heat absorbed by element

q_e = heat conducted through element in directior x

$$q_c = -k' t \frac{dT}{dx}$$

$$\frac{dq_c}{dx} = -k' t \frac{d^2T}{dx^2}$$

[1] $$k' t \frac{d^2T}{dx^2} dx = q_r - q_s$$

The heat radiated from the element can be designated as q_{ro} from the outside surface and q_{ri} from the inside surface. The quantity q_{ri} must include internal reflections. The same is true for q_s.

If the hole pattern is one that "averages" (as explained in Section 1.2.2) and is uniform around the circumference, the boom with holes can be replaced by an equivalent solid-wall boom with the following properties.

solar absorbtivity $= \alpha' = (1 - A_w)\alpha$

solar reflectivity $\rho' = (1 - A_w)\rho$

emissivity $= \epsilon' = (1 - A_w)\epsilon$

infrared reflectivity $\rho'_\epsilon = (1 - A_w)\rho_\epsilon$

transmissivity $\tau = A_w$

In order to account for inner reflections, the form factor from one element of the boom to another must be known. The form factor F_{1-2} from element dA_1 to dA_2 is given by (See Figure II-2):

$$F_{1-2} = \frac{\cos^2 \theta \, r \, d\theta \, dL}{\pi r'^2}$$

$$\cos \theta = \frac{r'}{2r}$$

$$F_{1-2} = \frac{d\theta \, dL}{4\pi r}$$

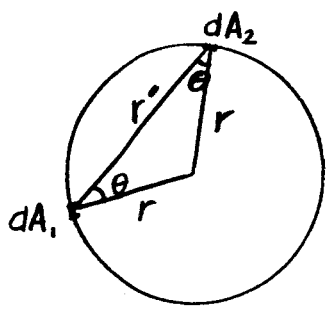

Figure II-2 Coordinate System For Form Factor

Since the form factor is not a function of θ, the heat radiated from any very long strip $Ld\theta_1$ to any other very long strip $Ld\theta_2$ is the same regardless of the angle between the strips. Thus for any diffuse internal reflection the reflected heat is uniformly distributed around the interior of the cylinder.

The net heat radiated by the interior surface of an element dx is determined as follows (See Figure II-3):

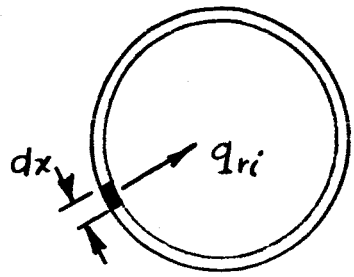

Figure II-3 Net Radiation From Interior Surface of Element dx

$$q_{ri}/dx = \epsilon'_i \sigma T_m^4 - \epsilon'_i (\epsilon'_i \sigma T_m^4) - \epsilon'_i \rho'_{\epsilon i} \sigma T_m^4 - \epsilon'^2_i \rho'^2_{\epsilon i} \sigma T_m^4 ---$$

$$\epsilon'_i \sigma T_m^4 \left[1 - \epsilon'_i - \epsilon'_i (\rho'_{\epsilon i} + \rho'^2_{\epsilon i} + --)\right]$$

$$\epsilon'_i \sigma T_m^4 \left[1 - \epsilon'_i (1 + \rho'_{\epsilon i} + \rho'^2_{\epsilon i} + ------)\right]$$

$$q_{ri}/dx = \epsilon'_i \sigma T_m^4 \left[1 - \frac{\epsilon'_i}{1 - \rho'_{\epsilon i}}\right]$$

The net heat absorbed by an element dx due to solar reflection is (See Figure II-4):

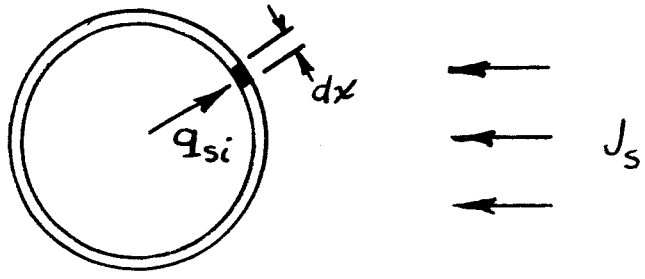

Figure II-4 Net Solar Reflected Radiation Absorbed by Element dx

$$q_{si} = \frac{J_s \tau}{\pi} \alpha'_i (+\rho'_i + \rho'^2_i + ------)$$

$$q_{si} = \frac{J_s \tau}{\pi} \left(\frac{\alpha'_i \rho'_i}{1 - \rho'_i}\right)$$

The heat inputs and outputs are different functions for the semi-circle near the sun, and the semi-circle away from the sun. They are:

For the semi-circle facing the sun

$$q_{so} = J_s \alpha'_o \cos x/r \, dx$$

$$q_{ro} = dx \sigma T_m^4 \epsilon'_o$$

$$q_{si} = J_s \tau \frac{\alpha'_i}{\pi} \left(\frac{\rho'_i}{1-\rho'_i}\right) dx$$

$$q_{ri} = \epsilon'_i \sigma T_m^4 \left(1 - \frac{\epsilon'_i}{1-\rho_{\epsilon'_i}}\right) dx$$

For the semi-circle away from the sun

$$q_{si} = J_s \, dx \, \tau \alpha'_i \left[-\cos x/r + \frac{1}{\pi}\left(\frac{\rho'_i}{1-\rho'_i}\right)\right]$$

$$q_{so} = 0$$

$$q_{ri} = \epsilon'_i \sigma T_m^4 \left(1 - \frac{\epsilon'_i}{1-\rho_{\epsilon'_i}}\right) dx$$

$$q_{ro} = \epsilon'_o \sigma T_m^4 \, dx$$

Substituting for q_r and q_s for each semicircle into [1]. For the near-sun side (Side 1) letting T_1 be the temperature on this side.

$$k' t \frac{d^2 T_1}{dx^2} dx = \sigma T_m^4 dx \left[\epsilon'_o + \epsilon'_i \left(1 - \frac{\epsilon'_i}{1-\rho_{\epsilon'_i}}\right)\right]$$

$$J_s \alpha'_o \cos x/r \, dx - J_s \tau \frac{\alpha'_i}{\pi}\left(\frac{\rho'_i}{1-\rho'_i}\right) dx$$

[2] Letting $\epsilon_i = \epsilon'_i \left(\frac{\epsilon'_i}{1-\rho_{\epsilon'_i}} - 1\right)$

and

[3] $$\alpha_i = \tau \frac{\alpha'_i}{\pi}\left(\frac{\rho'_i}{1-\rho'_i}\right)$$

$$k' t \frac{d^2 T_1}{dx^2} dx = \left\{\sigma T_m^4 \left[\epsilon'_o - \epsilon_i\right] - J_s \left[\alpha'_o \cos x/r + \alpha_i\right]\right\} dx$$

$$\frac{d T_1}{dx} = \frac{1}{k' t}\left\{\sigma T_m^4 \left[\epsilon'_o - \epsilon_i\right] x - J_s \alpha_i x - r J_s \alpha'_o \sin x/r + C_1\right\}$$

$$T_1 = \frac{1}{k' t}\left\{\frac{\sigma T_m^4}{2}\left[\epsilon'_o - \epsilon_i\right] x^2 - \tfrac{1}{2} J_s \alpha_i x^2 + r^2 J_s \alpha'_o \cos x/r + C_1 x + C_2\right\}$$

For the Far-sun side (Side 2) Letting T_2 be the temperature on this side.

q_r is the same whereas q_s is different

$$k't \frac{d^2T_2}{dx^2} dx = \sigma T_m^4 \left[\epsilon'_o - \epsilon_i\right] + J_s \tau \alpha'_1 \cos x/r - J_s \alpha_i \Big\} dx$$

$$\frac{dT_2}{dx} = \frac{1}{k't} \Big\{\sigma T_m^4 \left[\epsilon'_o - \epsilon_i\right] x - J_s \alpha_i x + r J_s \tau \alpha'_i \sin x/r + C_3 \Big\} dx$$

$$T_2 = \frac{1}{k't} \Big\{\frac{\sigma T_m^4}{2} \left[\epsilon'_o - \epsilon_i\right] x^2 - \tfrac{1}{2} J_s \alpha_i x^2 - r^2 J_s \tau \alpha'_i \cos x/r + C_3 x + C_4 \Big\} dx$$

The constants of integration can be determined by applying the following boundary conditions:

1. Continuous heat flow $(\frac{dT}{dx})$ and temperature T at $x = \frac{\pi r}{2}$ and $\frac{3\pi r}{2}$.
2. Zero heat flow at $x = 0$ and $x = \pi r$.

From (2) $$\left(\frac{d T_1}{dx}\right)_{(x=0)} = \left(\frac{d T_2}{dx}\right)_{x=\pi r} = 0$$

$$C_1 = 0$$

$$C_3 = -\sigma T_m^4 \pi r \left[\epsilon'_o - \epsilon_i\right] + J_s \alpha_i \pi r$$

From (1) $$\left(\frac{d T_1}{dx}\right)_{(x=\pi r/2)} = \left(\frac{d T_2}{dx}\right)_{(x=\pi r/2)}$$

$$- r J_s \alpha'_o \sin \pi/2 = +r J_s \tau \alpha'_i \sin \pi/2 - \sigma T_m^4 \pi r \left[\epsilon'_o - \epsilon_i\right] + J_s \alpha_i \pi r$$

$$J_s (-r\alpha'_o - r\tau\alpha'_i - \alpha_i \pi r) = -\sigma T_m^4 \pi r \left[\epsilon'_o - \epsilon_i\right]$$

$$J_s \alpha'_o + \tau \alpha'_i + \tau \alpha'_i \frac{\rho'_i}{1-\rho'_i}) = \pi \sigma T_m^4 \left[\epsilon'_o - \epsilon'_i \left(\frac{\epsilon'_i}{1-\rho'\epsilon_i} - 1\right)\right]$$

$$J_s \left[\alpha_o' + \tau\alpha_i' \frac{1}{1-\rho_i'}\right] = \pi\sigma T_m^4 \left[\epsilon_o' - \epsilon_i' \left(\frac{\epsilon_i (1-A_w)}{1-(1-\epsilon_i)(1-A_w)} - 1\right)\right]$$

$$J_s \left[\alpha_o' + \frac{\tau\alpha_i'}{A_w + \alpha_i (1-A_w)}\right] = \pi\sigma T_m^4 \left[\epsilon_o' + \frac{\epsilon_i' A_w}{A_w + \epsilon_i (1-A_w)}\right]$$

[4] $$T_m^4 = \frac{J_s \left[\alpha_o + \frac{A_w \alpha_i}{A_w + \alpha_i (1-A_w)}\right]}{\pi\sigma \left[\epsilon_o + \frac{A_w \epsilon_i}{A_w + \epsilon_i (1-A_w)}\right]}$$

This is the mean temperature of the boom.

From [1] $T_1 (x = \pi r/2) = T_2 (x = \pi r/2)$

$$C_2 = C_3 \pi r/2 + C_4$$

$$C_2 = -\sigma T_m^4 \frac{(\pi r)^2}{2} \left[\epsilon_o' - \epsilon_i\right] + J_s \alpha_i \frac{(\pi r)^2}{2} + C_4$$

The actual values of C_2 and C_4 cannot be determined by the Boundary Conditions directly, but only their relationship to one another. Substituting for the constants gives:

[5] $$T_1 = \frac{1}{k't} \left\{\frac{\sigma T_m^4}{2} \left[\epsilon_o' - \epsilon_i\right] (x^2 - \pi^2 r^2) - \tfrac{1}{2} J_s \alpha_i (x^2 - \pi^2 r^2) + r^2 J_s \alpha_o' \cos x/r + C_4\right\}$$

[6] $$T_2 = \frac{1}{k't} \left\{\frac{\sigma T_m^4}{2} \left[\epsilon_o' - \epsilon_i\right] (x^2 - 2\pi rx) - \tfrac{1}{2} J_s \alpha_i (x^2 - 2\pi rx) - r^2 J_s \tau\alpha_i' \cos x/r + C_4\right\}$$

NOTE: $C_4 \approx T_m$, however this has no relevance to the thermal bending.

To find the radius of curvature R of a boom with the temperature profile defined by equations (5) and (6), the elastic deflection of each element (dx) due to its temperature measured from a given datum temperature T is computed. It is then visualized that the elements are then forced to assume their original length, then all allowed to expand some equal amount A, and then the boom is allowed to bend to a curvature $\frac{1}{R}$ so that each element strains according

to the equation $\frac{r}{R}\cos x/r$. Thus the total deflection of each element from the unrestrained expansion is

$$\delta = e\,T + A + r/R \cos x/r.$$

The energy expended on the boom in this deflection is

$$\mathcal{E} = 2\left[\tfrac{1}{2}\int_0^{\pi r} \delta^2 E\,dx\,t\right]$$

per unit length, and is also the elastic energy stored in the boom.

If this term is computed and the derivative with respect to $(\frac{1}{R})$ computed and set to zero, this will give the value of $\frac{1}{R}$ for which the elastic energy is a minimum and thus will give the actual radius of curvature assumed (since an object always assumes the shape of minimum elastic energy).

Expanding the last equation and dropping all terms not including R gives

$$\mathcal{E} = Et\left\{\int_0^{\pi r} 2\,e\,T\,r/R\cos x/r\,dx + 2\,A\,r/R\cos x/r\,dx + (\tfrac{r}{R})^2\cos^2 x/r\,dx\right\}$$

[7]
$$\mathcal{E} = Et\left\{\int_0^{\pi r/2} 2\,e\,T_1\,r/R\cos x/r\,dx + \int_{\pi r/2}^{\pi r} 2\,e\,T_2\,r/R\cos x/r\,dx + \int_0^{\pi r} 2A\,r/R\cos x/r\,dx + (\tfrac{r}{R})^2\cos^2 x/r\,dx\right\}$$

To simplify the following operations, equations [5] and [6] can be written as

$$T_1 = A_1 x^2 - A_1 \pi^2 r^2 - A_2 x^2 + A_2 \pi^2 r^2 + A_3 \cos x/r + A_4$$

$$T_2 = A_1 x^2 - A_1\, 2\pi rx - A_2 x^2 + 2\,A_2\,\pi rx - A_5 \cos x/r + A_4$$

where

$$A_1 = \frac{1}{kt}\,\frac{\sigma\,T_m^4}{2}\left[\epsilon'_o - \epsilon_i\right]$$

$$A_2 = \frac{1}{2kt}\,J_s\,\alpha_i$$

$$A_3 = \frac{1}{kt}\,r^2\,J_s\,\alpha'_o$$

$$A_4 = \frac{1}{kt}\ C_4$$

$$A_5 = \frac{1}{kt}\ r^2\ J_s\ \tau \alpha_i'$$

Substituting for T_1 and T_2 into (7)

$$\mathcal{E} = Et\ 2e\ r/R \int_o^{\pi r/2} A_1\ x^2 \cos x/r\ dx - A_1 \pi^2\ r^2 \cos x/r\ dx$$

$$- A_2\ x^2 \cos x/r\ dx + A_2 \pi^2\ r^2 \cos x/r\ dx + A_3 \cos^2 x/r\ dx + A_4$$

$$\cos x/r\ dx + E\ t2e\ r/R \int_{\pi r/2}^{\pi r} + A_1\ x^2 \cos x/r\ dx - A_1\ 2\pi rx \cos x/r$$

$$dx - A_2\ x^2 \cos x/r\ dx + 2A_2 \pi\ rx \cos x/r\ dx - A_5 \cos^2 x/r\ dx +$$

$$A_4 \cos x/r\ dx + \left\{ \int_o^{\pi} \frac{A}{e} \cos x/r\ dx + \int_o^{\pi} \frac{r}{2eR} \cos^2 x/r\ dx \right\}$$

$$\mathcal{E} = 2\ E\ te\ r/R \left\{ \int_o^{\pi r} x^2 \cos x/r\ (A_1 - A_2)\ dx + \int_o^{\pi r/2} \cos x/r \right.$$

$$(-A_1 \pi^2\ r^2 + A_2 \pi^2\ r^2)\ dx + \int_o^{\pi r} A_4 \cos x/r\ dx + \int_o^{\pi r/2} A_3 \cos^2$$

$$x/r\ dx - \int_{\pi r/2}^{\pi r} (A_1\ 2\pi r - A_2\ 2\pi r)\ x \cos x/r\ dx +$$

$$\int_{\pi r/2}^{\pi r} - A_5 \cos^2 x/r\ dx + \int_o^{\pi r} \frac{A}{e} \cos x/r\ dx + \int_o^{\pi} \frac{1}{2e}\ r/R \cos^2$$

$$\left. x/r\ dx \right\}$$

$$\mathcal{E} = 2\ E\ te\ r/R \left\{ r^3\ (A_1 - A_2) \left[2\beta \cos\beta + (\beta^2 - 2) \sin\beta \right]_o^{\pi} \right.$$

$$+\pi^2\ r^3\ (A_2 - A_1) \left[\sin\beta \right]_o^{\pi/2} + r\ A_3 \left[\tfrac{1}{2}\beta + \tfrac{1}{4} \sin 2\beta \right]_o^{\pi/2}$$

$$- 2\pi r^3\ (A_1 - A_2) \left[\cos\beta + \beta \sin\beta \right]_{\pi/2}^{\pi} - A_5\ r \left[\tfrac{1}{2}\beta + \tfrac{1}{4} \sin 2\beta \right]_{\pi/2}^{\pi}$$

$$\left. + \frac{1}{2e}\ r^2/R \left[\tfrac{1}{2}\beta + \tfrac{1}{4} \sin 2\beta \right]_o^{\pi} \right\}$$

$$\mathcal{E} = 2\,E\,te\,r/R\left\{r^3\,(A_1 - A_2)\,(-2\pi) + \pi^2\,r^3\,(A_2 - A_1) + r\,A_3\,\pi/4 + 2\,\pi r^3\,(A_1 - A_2)\,(1 + \pi/2) - A_5\,r\,\pi/4\right\} + \frac{Et\pi r}{2}\,(r/R)^2$$

$$\mathcal{E} = K_1\left(\frac{1}{R}\right) + K_2\,\frac{1}{R^2}$$

$$\frac{\partial \mathcal{E}}{\partial R} = -K_1\,\frac{1}{R^2} - 2K_2\,\frac{1}{R^3} = 0$$

$$-K_1 = 2K_2\,\frac{1}{R}$$

$$\frac{1}{R} = -\frac{K_1}{2K_2}$$

$$K_1 = 2\,E\,te\,r\left\{A_1 + A_2 + (A_3 - A_5)\,\pi r/4\right.$$

$$K_2 = \frac{Et\pi}{2}\,r^3$$

$$\frac{1}{R} = -\frac{2e}{r}\left[+\,(A_3 - A_5)\,\pi/4\right]$$

$$\frac{1}{R} = \frac{2e}{r}\,\frac{A_3 - A_5}{4}$$

$$\frac{1}{R} = \frac{2er}{k't}\,\frac{J_s\,(\alpha_o' - \tau\,\alpha_i')}{4}$$

$$\frac{1}{R} = \frac{er\,J_s}{2\,k't}\,(\alpha_o' - \tau\,\alpha_i')$$

For solar radiation at an angle θ from the boom axis

[8] $$\frac{1}{R} = \frac{er\,J_s}{2\,k't}\,\sin\theta\,(1 - A_w)\,(\alpha_o - A_w\,\alpha_i)$$

For earth radiation at an angle θ to the boom axis (when the radiation can be considered collimated) the curvature is given by

[9] $$\frac{1}{R} = \frac{er\,J_E\,\sin\theta}{2\,k't}\,(1 - A_w)\,(\epsilon_o - A_w\,\epsilon_i)$$

Note that this latter bending will be zero if $\epsilon_o = A_w \epsilon_i$ even if the radiation is <u>not</u> considered collimated.

APPENDIX III

INFLUENCE OF SEAM CONDUCTIVITY ON THERMAL BENDING

In Section 1.2.2.2, assumption (4) is stated, the assumption being that the seam has the same conductivity as the rest of the boom. Of course, this is not actually the case, so it is important to consider the effects of the seam having poor conduction. The following facts can be stated.

1) The fractional window area, A_w, is the same at the seam as elsewhere, so that the seam has little or no effect on the shadowing or distribution of irradiation.

2) If the seam is at $\beta = 0°$ or 180°, no heat is conducted across it, so it has no effect.

3) If the seam is at 90° or 270°, and if $\alpha_o = A_w \alpha_i$, no heat is conducted across it, so it has no effect.

4) For the design where $\alpha_o = A_w \alpha_i$, the maximum effect of the seam occurs where dT/dx is a maximum.

To estimate the worst possible effect of poor seam conductivity for the design where $\alpha_o = A_w \alpha_i$, let us assume that the seam conductivity is zero, and that the seam is at such an angle β from the sun line that dT/dx is a maximum at the seam. This angle β ($\beta = x/r$) is found as follows:

Setting $\frac{d^2T_1}{dx^2} = 0$, from Section 1.2.2.2 we get $J_s \left[\frac{\alpha_o' + \tau \alpha_i'}{\pi} + \alpha_i\right]$

$= J_s \left[\alpha_o' \cos x/r + \alpha_i\right]$

Substituting for α_o' and $\tau \alpha_i'$, and solving for cos x/r gives

$\cos x/r = 2/\pi\tau$

$\beta = x/r = 50.5° = .882$ radians

NOTE: Other angles are β = 129.5°, 230.5°, and 309.5°.

The temperature gradient at this point is

$$\left(\frac{dT_1}{dx}\right) = \frac{1}{k't} \left\{\sigma T_m^4 \left[\varepsilon_o' - \varepsilon_i\right] x - J_s \alpha_i x - r J_s \alpha_o' \sin x/r\right\}$$

$$\frac{dT_1}{dx} = \frac{J_s}{k't} \left\{ \left[\frac{\alpha_o' + \tau \alpha_i'}{\pi} + \alpha_i' \right] x - \alpha_i' x - r \alpha_o' \sin x/r \right\}$$

For

$$\alpha_o' = \tau \alpha_i'$$

$$\frac{dT_1}{dx} = \frac{J_s}{k't} \left\{ \alpha_o' \left(\frac{2x}{\pi} - r \sin x/r \right) \right\}$$

At $x/r = 50.5°$ and for $r = .25$, $x/r = .882$, $x = .882\ r$

$$\frac{dT_1}{dx} = \frac{J_s}{k't} (-.053\ \alpha_o')$$

To choose a specific example for quantitative values, assume the following:

$$\alpha_o' = \tau \alpha_i' = .07$$

$$\tau = A_w = .07 \therefore \alpha_i = 1 \text{ and } \alpha_i' = 0$$

$k' = .90\ k = .90\ (3.67) = 3.30$, Btu/hr in°F

$t = .002$ inches

$J_s = 3.12$ Btu/hr in^2

$$\frac{dT_1}{dx} = \frac{3.12}{3.30\ (.002)} \left\{ -.053\ (.07) \right\}$$

$$\left(\frac{dT_1}{dx} \right)_{\beta = 50.5°} = 1.75\ °F/in. \text{ at the seam}$$

Now, because these equations are linear for small ΔT ($\frac{\Delta T}{T_m} << 1$), the principal of superposition can be employed. If a heat flow q, in the opposite direction to that in the analtyical solution, is superposed of such a magnitude that $q_1 = k't \left(\frac{dT}{dx}\right)_{\beta = 50.5°}$ as illustrated in Figure III-1.

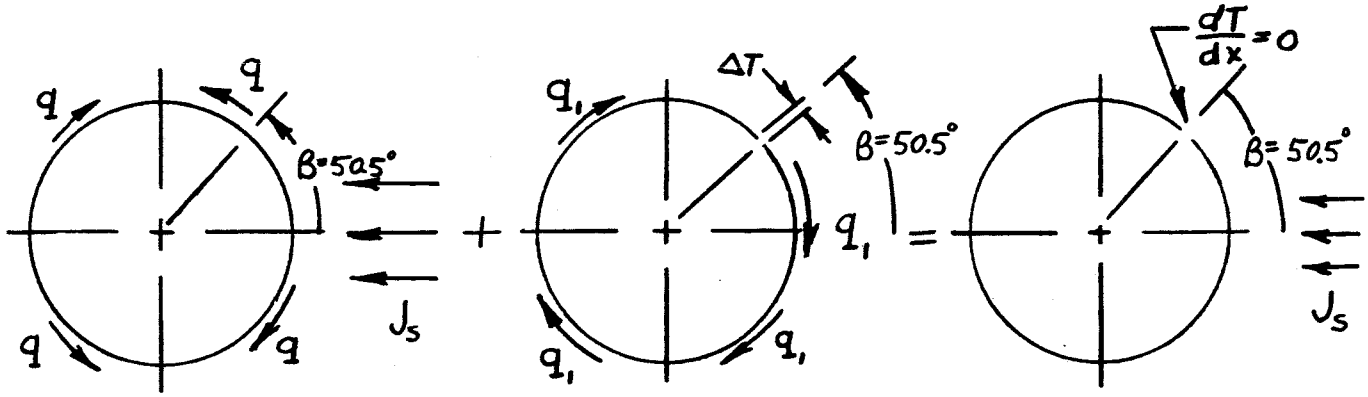

Seamless boom with q determined by Appendix I.

Boom with non-conducting seam with constant flow q_1

Boom with non-conducting seam and solar irradiation.

Figure III-1 Superposition of Heat Flows For No Heat Flow at Seam

then the temperature drop ΔT across the seam is given by

$$\Delta T = \int_{x=0}^{x=2\pi r} \frac{dT}{dx}$$

$$\Delta T = \left(\frac{dT}{dx}\right)_{\beta = 50.5^\circ} 2\pi r$$

$$\Delta T = 2.75^\circ F$$

Since the seam can carry shear forces, the differential expansion due to ΔT cannot occur across the seam. However thermal bending will occur about a diametral axis through the seam with the bending away from the sun side. The magnitude of bending can be determined exactly by energy methods but is given approximately by

$$\frac{1}{R} = \frac{e \Delta T_{AV}}{2r} = \frac{e \Delta T_{seam}}{4r}$$

$$\frac{1}{R} = \frac{1.04 \cdot 10^{-5} (2.75)}{4 (.25)} \text{ in}^{-1}$$

$$\frac{1}{R} = 2.86 \cdot 10^{-5} \text{ in}^{-1}$$

For a 30-inch cantilevered boom, this is equivalent to a tip deflection of .013 inches.